A Third Neanderthal Individual from La Ferrassie Dated to the End of the Middle Palaeolithic

Guillaume Guérin, Vera Aldeias, Frederik Baumgarten, Paul Goldberg, Asier Gómez-Olivencia, Christelle Lahaye, Stéphane Madelaine, Bruno Maureille, Anne Philippe, Dennis Sandgathe, et al.

A Third Neanderthal Individual from La Ferrassie Dated to the End of the Middle Paleolithic

GUILLAUME GUÉRIN*
Université Rennes, CNRS, Géosciences Rennes, UMR 6118, 35000 Rennes, FRANCE; guillaume.guerin@univ-rennes1.fr

VERA ALDEIAS
Interdisciplinary Center for Archaeology and Evolution of Human Behaviour (ICArEHB), FCHS, University of Algarve, Faro, PORTUGAL; vlaldeias@ualg.pt

FREDERIK BAUMGARTEN
Department of Physics, Technical University of Denmark, DTU Risø Campus, Roskilde, DENMARK; fhaba@dtu.dk

PAUL GOLDBERG
Institute for Archaeological Sciences, University of Tübingen, 72074 Tübingen, GERMANY; and, SEALS, University of Wollongong, Wollongong, NSW 2522, AUSTRALIA; paulberg@bu.edu

ASIER GÓMEZ-OLIVENCIA
Departement Geología, Universidad del País Vasco/Euskal Herriko Unibertsiatea (UPV/-EHU), Barrio Sarriena s/n, 48940 Leioa; Sociedad de Ciencias Aranzadi, Zorroagagaina 11, 20014 Donostia-San Sebastian; and, Centro UCM-ISCIII de Investigación sobre Evolución y Comportamiento Humanos, Avda. Monforte de Lemos 5 (Pabellón 14), 28029 Madrid, SPAIN; asiergo@gmail.com

CHRISTELLE LAHAYE
Archéosciences Bordeaux, UMR 6034 CNRS - Université Bordeaux Montaigne, Maison de l'archéologie, Esplanade des Antilles, 33607 Pessac cedex, FRANCE; christelle.lahaye@u-bordeaux-montaigne.fr

STÉPHANE MADELAINE
Musée national de Préhistoire, F-24620 Les Eyzies-de-Tayac; and, Université Bordeaux, CNRS, MC, PACEA UMR 5199, F-33600 Pessac, FRANCE; stephane.madelaine@culture.gouv.fr

BRUNO MAUREILLE
Université Bordeaux, CNRS, MC, PACEA UMR 5199, F-33600 Pessac, FRANCE; bruno.maureille@u-bordeaux.fr

ANNE PHILIPPE
Jean Leray Laboratory of Mathematics (LMJL), UMR 6629 CNRS - Université de Nantes, Nantes, FRANCE; anne.philippe@univ-nantes.fr

DENNIS SANDGATHE
Human Evolution Studies Program and Department of Archaeology, Simon Fraser University, Burnaby, CANADA; dmsandga@gmail.com

SAHRA TALAMO
Department of Chemistry, University of Bologna, Bologna, ITALY; sahra.talamo@unibo.it

KRISTINA JØRKOV THOMSEN
Department of Physics, Technical University of Denmark, DTU Risø Campus, Roskilde, DENMARK; krth@dtu.dk

ALAIN TURQ
Musée national de Préhistoire, F-24620 Les Eyzies-de-Tayac; and, Université Bordeaux, CNRS, MC, PACEA UMR 5199, F-33600 Pessac, FRANCE; alain.turq@orange.fr

ANTOINE BALZEAU
Équipe de Paléontologie Humaine, UMR 7194, CNRS, Département Homme et environnement, Muséum national d'Histoire naturelle, Musée de l'Homme, 17 Place du Trocadéro, 75016 Paris, FRAMCE; and, Department of African Zoology, Royal Museum for Central Africa, Tervuren, BELGIUM; antoine.balzeau@mnhn.fr

Corresponding author: Guillaume Guérin; *guillaume.guerin@univ-rennes1.fr*

submitted: 3 November 2022; revised: 7 March 2023; accepted: 8 March 2023

Handling Editor in Chief: Erella Hovers

***PaleoAnthropology* 2023:1: 98–118.** **https://doi.org/10.48738/2023.iss1.811** **ISSN 1545-0031**

ABSTRACT

The Paleolithic site of La Ferrassie (SW France) has been extensively studied since its discovery during the 19th century. In addition to a large sequence including Middle and Upper Paleolithic layers, the site has yielded two very complete adult Neanderthal skeletons, five partial immature Neanderthal skeletons as well as a few isolated human remains. Currently, much of the site sequence has been dated by radiocarbon and OSL but the dating of the human skeletal remains is still a matter of debate. Here, we present the OSL dating of a still consolidated sediment sample associated with the Neanderthal skeleton La Ferrassie 1 (LF1), unearthed by Peyrony and Capitan in 1909 and preserved at the Musée de l'Homme (Paris, France). This block of sediment is crucial as it constitutes the first possibility to date a sample in close association with the specimen. This sample is included in a chronological model at the scale of the site, with the aim to estimate the ages of three Neanderthal individuals: La Ferrassie 1, 2, and 8 (LF1, LF2 and LF8). Two chronological modelling tools (OxCal and BayLum/ArchaeoPhases) are first applied to previously published radiocarbon ages and compared. Chronological inferences show that the BayLum/ArchaeoPhases model provides posterior probability densities, or statistical inferences, that are more consistent with the measured data. When including OSL ages in the BayLum model, we can conclude that all three studied individuals date from the late Middle Paleolithic (<52 ka at the 95% credibility level) and could have been contemporaries some time 44.9 and 44.1 ka ago.

INTRODUCTION

The site of La Ferrassie (Savignac-de-Miremont, SW France) is famous for a long sequence of Middle and Upper Paleolithic archaeological layers (Capitan and Peyrony, 1912a; Peyrony, 1934; Delporte et Tuffreau, 1973; Delporte and Delibrias, 1984). In addition, Peyrony and Capitan unearthed several isolated human remains as well as parts of six Neanderthal individuals in the early XXth century (LF1-6 (Capitan and Peyrony, 1909, 1912b), while Delporte revealed a seventh in 1970 and 1973 (La Ferrassie 8, LF8). These seven individuals represent different ages at death, from one foetus to at least two middle age adults (Heim, 1976, 1982a, 1982b). In 2010, an international team undertook new excavations of the site to re-evaluate the archaeological remains of the different layers, establish a numerical chronology for the sequence and provide as much contextual information as possible on the human remains. Figure 1 shows an overview of the site, its different sectors, and the approximate location of the three skeletons investigated in this work: La Ferrassie 1, 2, and 8 (LF1, LF2 and LF8).

Thus far, the main sequence has been dated (Guérin et al., 2015; Talamo et al., 2020) by a combination of Optically Stimulated Luminescence (Huntley et al., 1985; Murray et al., 2021) and radiocarbon (Hajdas et al., 2021) methods. By examining sediment still attached to the foot of LF2, we could correlate it with—most likely—our Layer 5, although our Layer 4 could not be excluded (the reader is referred to Guérin et al. [2015], for the correspondence between Peyrony's layers and ours). As a consequence, by dating Layer 5 Guérin et al. (2015) proposed an age of ~43–45 ka for this individual, with an upper limit of no more than 54±4 ka.

New human fossil remains were found in 2013 among indeterminate fragments from the sector where LF 8 was found (Gómez-Olivencia et al., 2015). These findings led to new excavations in the La Ferrassie 8 sector. A dating campaign involving radiocarbon and OSL provided a number of radiocarbon ages for samples associated with this young infant (Balzeau et al., 2020). One Neanderthal bone, identified by mitochondrial DNA, was dated among the radiocarbon samples. It is currently not demonstrated that this bone belongs to LF 8 in absence of direct anatomical correspondence, as this particular sample is an undefined bone fragment; however, all the elements that were anatomically identifiable in this area share a developmental stage and represent anatomical parts that are fully compatible with the presence of a unique individual. Nevertheless, considering the discrepancy between radiocarbon and adjacent OSL ages, together with a taphonomic study of the archaeological remains in this area, Balzeau et al. (2020) claimed that the LF 8 Neanderthal possibly had been buried.

Here, we present new data regarding the age of a third individual: LF 1. This skeleton was unearthed by Peyrony and Capitan in 1909 (Capitan and Peyrony, 1909) and removed within a block of sediment for transportation in the Musée de l'Homme. There, it was excavated by paleontologist J. Piveteau. According to Peyrony and Capitan, LF 1 was found very close to, and within the same stratigraphic unit as, LF2 (but the excavation standards at the time preclude us from determining this conclusively). The area where the specimen was discovered was completely dug out. It is therefore no longer possible to analyse the sedimentary context of the fossil directly in the site. However, D. Peyrony and M. Boule observed small packets of yellow sand from the lower level mixed with the Mousterian sediments associated with both LF1 and LF2 (Maureille and Van Peer, 1998). This is something that was not observed in the rest of the Mousterian levels and was interpreted as the effect of intentional funerary pits. These pits removed sediment from the underlying level and mixed this sediment with that which later filled the pit (Maureille and Van Peer, 1998). Moreover, according to a taphonomic analysis, no surface alteration is present in the LF1 skeleton and the breakage pattern is that of bone that has lost collagen, which would be consistent with the intentional burial of this individual (Gómez-Olivencia et al., 2018).

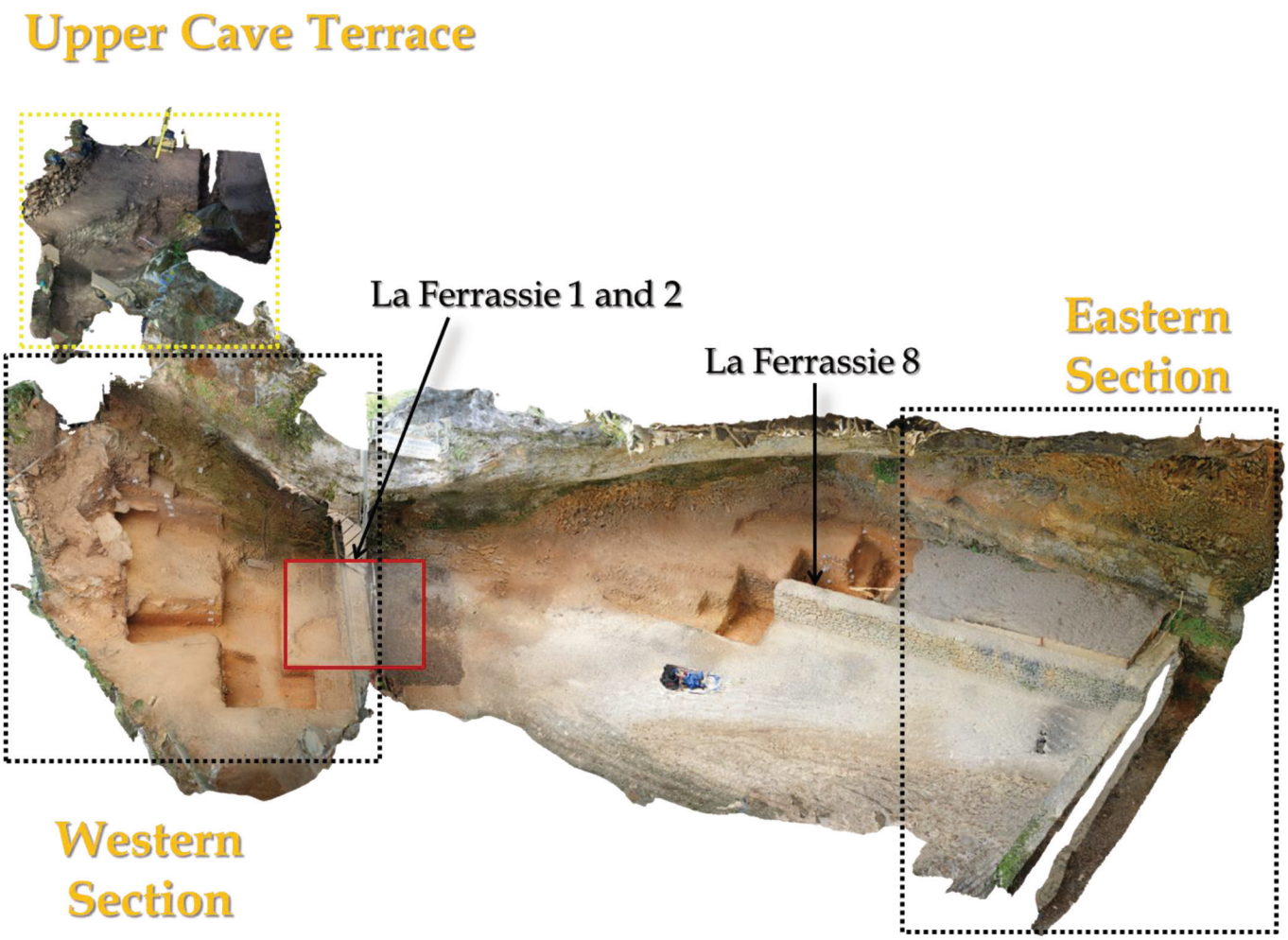

Figure 1. View of the different sectors of La Ferrassie. The Western section is referred to as the main section in the text. The circular feature inside the red square corresponds to the pit dug by excavators in the early 1900s to remove La Ferrassie 2 with a block of sediment. La Ferrassie 1 was found close to it. Finally, La Ferrassie 8 was found by Delporte in the early 1970s, close to the wall of the Grand Abri.

Knowledge of the chronology of the human remains found at the site is very limited and mostly based on rare evidence and general considerations. For example, Heim (1982a, b) concluded that all the human remains are evidently contemporaneous. Moreover, this scholar then considered that they would be dated from the end of the Mousterian, around 35 000 years ago, according to attempts of ^{14}C dating. However, the published age (Delibrias, 1984) for the Mousterian layer is >35 000 years ago. A more recent analysis of a bone coming from an Aurignacian layer of the site (excavated by Delporte in 1972 and originally dated by Mellars et al., 1987) provided an uncalibrated radiocarbon age of 33,610 BP (Higham et al., 2006), but the latter estimate was still believed to underestimate the true age. The two tibias of LF 1 were later sampled for direct dating (Higham et al., 2014), but once again the authors concluded that contamination makes the obtained ages erroneous. An age around 70,000 ya for the human remains is often mentioned (e.g., Mellars, 1996, who placed Ferrassie Mousterian before Quina Mousterian, and thus around 70 ka), even if the scientific evidence on which this age is based is not very clear. In fact, the chronological context of most of the Neanderthal fossils from La Ferrassie is not yet based on direct and robust evidence.

Luckily, by exploring the collections of the Musée de l'Homme, we found some sediment associated with LF 1; part of this sediment was still consolidated by calcite cementation. In this work, we present the OSL dating of this new sediment sample attached to LF1, then Bayesian modelling of the chronology established for LF1, LF2 and LF8. For this purpose, we use the open-source, specifically-designed software BayLum (Combès et al., 2015; Combès and Philippe, 2017; Philippe et al., 2019; Christophe et al., 2020; Guérin et al., 2021; 2022), which allows age calculations by combining radiocarbon and OSL measurements, while including stratigraphic constraints and shared errors affecting the OSL measurements.

MATERIALS AND METHODS

PREVIOUSLY PUBLISHED AGES

Many data used in this study have already been published in Guérin et al. (2015), Talamo et al. (2020), and Balzeau et al. (2020). In particular, we consider that LF2 is dated by the most likely association with Layer 5 or possibly Layer 4 (Guérin et al., 2015) and that LF8 is bracketed by the radiocarbon ages obtained on organic material associated to this skeleton (Balzeau et al., 2020). Another possibility for LF8 would be that its age corresponds to that determined by radiocarbon on the Neanderthal remain dated by Balzeau et al. (2020).

Not all OSL and radiocarbon ages obtained from La Ferrassie are included in this study, because not all dated samples are relevant. Indeed, we excluded the following samples from the present study:

- OSL sample FER 2, coming from Layer 6 in the main excavation sector, was omitted from the present study because it was shown by Guérin et al. (2015) to be poorly-bleached. The modelling software BayLum, used in the following, does not include minimum age modelling. However, it should be noted here that this sample is not crucial for our analyses, since many radiocarbon samples are available for this layer, and since both OSL and radiocarbon samples are available directly above and below Layer 6;
- The four OSL samples taken adjacent to the find location of LF8 are also omitted, because they were shown by Balzeau et al. (2020) to be much older than LF8 itself. The apparent disagreement between OSL and radiocarbon led Balzeau et al. (2020) to suggest that this child was buried in a pit, since more recent archaeological material was found at the same elevation as LF8. In other words, the OSL ages from this area are unrelated to the age of LF8. Hence, because the present study is focused on the age of the skeletons, the four OSL samples from this area are irrelevant in this context;
- All radiocarbon samples identified as outliers by Talamo et al. (2020: Figure 3) were also excluded; in particular, all radiocarbon samples from Layer 4, identified as outliers in this article, were removed as well for the present study;
- Finally, all radiocarbon samples from Layer 3 were excluded because they are too old; indeed, this layer is dated beyond the range of IntCal20 (Reimer et al., 2020).

On the other hand, we include all OSL samples from the main excavation area (except poorly bleached sample FER2) in our chronological modelling. While Layers 1 and 2 are significantly older than Layers 4 and 5 where LF2 was found, we decided to include the corresponding samples because we derive the site's chronology using stratigraphic constraints and our knowledge of systematic errors affecting the OSL age measurements. Although of secondary importance for the present study, based on post Infra-Red Infra-Red Stimulated Luminescence (pIRIR), Frouin et al. (2017) suggested that the OSL ages of Guérin et al. (2015) might underestimate the true deposition ages for Layers 1 and 2, due to early saturation of the OSL signal for these two layers. Including the OSL samples from these layers might help solve this issue, since BayLum appears to be less sensitive to saturation effects than conventional analyses (e.g., Heydari and Guérin, 2018).

For an overview of the sample list, Table 1 contains all already published ages that are relevant to the present study, i.e. 13 OSL and 33 radiocarbon samples.

NEW OSL SAMPLE

The only additional sample compared to previous studies comes from a block of naturally consolidated sediment associated with LF1 and preserved at the Musée de l'Homme (Figure 2) in boxes, with the label corresponding to La Ferrassie 1 in the entries of the collections catalogue. The hominin material was taken from the site of La Ferrassie in the form of three large blocks consolidated with plaster and containing the different parts of the skeleton. The detailed excavation of those blocks was performed in the Museum national d'Histoire naturelle. Some faunal remains, lithic elements, and some pieces of sediment that were associated with the human remains in the blocks have been preserved in the collection. That is why we could gain access to the chunk of sediment that has been preserved as a block during the preparation of the skeleton. We have no information allowing us to know in which block of plaster this piece of sediment was. Nevertheless, we know, thanks to the famous photograph showing the skeleton in place at the site, that all the sediment that covered it had been removed. The plaster blocks bordered the human remains on the sides, so that their size was minimal in relation to the surface on which the bones were exposed. In this context, we know that the block of sediment was near the skeleton, no more than 20 to 30 centimeters away from the human bones and possibly in contact with them (see Supplementary Material).

During sampling, one of us (PG), who worked on the sediment of La Ferrassie, examined the sediment sample with a hand lens and concluded that it looks just like that from our Layer 5—compact yellowish red brown silty sand with abundant cm-sized fragments of lithics and bone (it should be noted here that no other layer presents these features: see Table 1 of Guérin et al., 2015). Given the potentially interesting information contained in this block, we only sampled a small part of it. First, we consolidated the targeted part of the block with plaster bands, to prevent the sediment from disaggregating. In subdued orange lighting, we removed the targeted sub-block from the main body of sediment. Our sample was then placed in an opaque bag and transported to the Archeosciences Laboratory in Bordeaux, where the sediment was carefully extracted from the consolidated block. Special care was taken not to include grains from the edge (~1cm from the surface) to avoid sampling grains that would have been exposed to light in the Museum or during original sampling of LF in the early XXth century.

TABLE 1. OSL AND UNCALIBRATED RADIOCARBON AGES RELEVANT FOR THIS STUDY AND PUBLISHED BY GUÉRIN ET AL. (2015), TALAMO ET AL. (2020), AND BALZEAU ET AL. (2021).

Layer	Sample*	Age (ka)
Main sequence		
9	MAMS-25529 (^{14}C)	27.1±0.2
	MAMS-25530 (^{14}C)	25.1±0.1
8	MAMS-25527 (^{14}C)	26.3±0.1
	MAMS-25528 (^{14}C)	27.2±0.2
7	FER1 (OSL)	39.9±2.5
	MAMS-16376 (^{14}C)	39.1±0.2
	MAMS-25520 (^{14}C)	33.1±0.3
	MAMS-25521 (^{14}C)	32.5±0.2
	MAMS-16374 (^{14}C)	32.6±0.2
	MAMS-16377 (^{14}C)	33.0±0.2
	MAMS-25525 (^{14}C)	32.8±0.3
6	MAMS-16373 (^{14}C)	37.4±0.4
	MAMS-25522 (^{14}C)	36.6±0.4
	MAMS-25523 (^{14}C)	39.0±0.5
	MAMS-25524 (^{14}C)	40.8±0.7
	MAMS-21206 (^{14}C)	40.9±0.5
5	FER3 (OSL)	42.5±3.1
	FER4 (OSL)	46.0±3.7
	FER14-MG (OSL)	44.8±2.7
	MAMS-17580 (^{14}C)	41.7±0.3
	MAMS-17582 (^{14}C)	43.5±0.4
	MAMS-17581 (^{14}C)	42.4±0.3
	MAMS-16372 (^{14}C)	42.4±0.7
	MAMS-16371 (^{14}C)	42.1±0.7
	MAMS-16381 (^{14}C)	43.4±0.3
	MAMS-17583 (^{14}C)	42.0±0.3
4	FER5-MG (OSL)	46.2±2.7
	FER6-MG (OSL)	56.5±3.5
3	FER8-MG (OSL)	54.3±2.9
	FER13-MG (OSL)	46.1±2.6
	FER7 (OSL)	63.2±4.0
2	FER9 (OSL)	74.2±5.3
	FER10-MG (OSL)	64.9±4.0
1	FER11-MG (OSL)	90.1±7.4
	FER12-MG (OSL)	95.1±9.0

EXPERIMENTS, MISSING INFORMATION AND DATA ANALYSIS

The LF1 sample was measured using the single-grain OSL measurement protocols employed by Guérin et al. (2015) for their La Ferrassie samples. The single-grain OSL signals were measured using an automated Risø TL/OSL DA 20 reader by individual stimulation with a green laser beam (Duller, 1999; Bøtter-Jensen et al., 2000) and detected through a UV filter set. Environmental beta dose rates were determined by high-resolution gamma spectrometry of the outer part of the block of sediment. All factors used to account for water absorption in sediment, grain size attenuation of beta dose rates, internal dose rate, etc., are the same as in Guérin et al. (2015). Only the laboratory dose rates were changed—because the dose delivered to the Risø calibration quartz was re-estimated, changing from 4.81 to 5

TABLE 1. OSL AND UNCALIBRATED RADIOCARBON AGES RELEVANT FOR THIS STUDY AND PUBLISHED BY GUÉRIN ET AL. (2015), TALAMO ET AL. (2020), AND BALZEAU ET AL. (2021) (continued).

Layer	Sample*	Age (ka)
Main sequence		
LF8 area	MAMS-27340 (^{14}C)	40.7±0.3
	MAMS-29545 (^{14}C)	41.8±0.3
	MAMS-29546 (^{14}C)	37.7±0.3
	MAMS-27341 (^{14}C)	41.3±0.4
	MAMS-27342 (^{14}C)	34.8±0.2
	MAMS-29547 (^{14}C)	39.2±0.2
	MAMS-29548 (^{14}C)	42.4±0.3
	ETH-99102 (^{14}C)	36.2±0.2
	ETH-99103 (^{14}C)	35.4±0.2
	ETH-99104 (^{14}C)	37.7±0.3
	ETH-99105 (^{14}C)	40.6±0.4

*Samples whose names start with 'MAMS' or 'ETH' are radiocarbon samples; all others are OSL samples, measured either as single-grains or as multi-grains (in the latter case, the sample name ends with 'MG'). Note: all OSL ages are 4% older than in Guérin et al. (2015) because of a re-estimation of the dose to calibration quartz (see text for details).

Gy (Hansen et al., 2015; Richter et al., 2020; Murray, pers. comm. to Guérin).

However, the sediment surrounding the sample during burial at the gamma dose rate scale (30–50cm: Guérin and Mercier, 2011) was excavated in the early XXth century, so it was impossible to measure *in situ* gamma dose rates. Whereas such measurements are not necessarily required when working in homogeneous contexts, gamma dose rates are highly variable at La Ferrassie—not only when approaching the bedrock walls but also from one layer to the other. As a result, we had to estimate the appropriate gamma dose rate that the LF1 sediment sample was exposed to, based on independent information. To this end, we used the following sentence from Capitan and Peyrony (1912a) describing the relative position of the skeletons: '*Quant au second squelette, il fut découvert en septembre 1910. Il gisait en plein milieu de la couche moustérienne et plutôt même dans sa moitié inférieure, à 1 m. 50 de la paroi rocheuse et à 0 m. 50 seulement du précédent*' ('Regarding the second skeleton, it was found in September, 1910. It was lying in the middle of the Mousterian layer, more precisely in its lower half, 1.50m away from the cave wall and only 0.50m away from the previous one'). Based on sedimentological observations, Guérin et al. (2015) attribute the latter to most likely Layer 5, and so we decided to use the average of the gamma + cosmic dose rates measured for this layer as our best estimate of that experienced by the LF1 sediment sample. For the corresponding uncertainty, we used the standard deviation of all dose rate measurements from Layer 5 (rather than the standard error of the mean, since the single value relevant for LF1 could lie in the entire range of all measured values). As a result, the gamma dose rate for LF1 is estimated to be 0.39±0.17 Gy.ka^{-1}; the large uncertainty (44%) reflects our poor knowledge of the sample's burial environment. However, with this cautious approach we can be confident that the true gamma dose rate lies within two standard errors of the central value, since the corresponding interval includes all gamma dose rate values measured at the site and in particular the dose rate estimated for our samples from Layer 4 (0.49±0.07 Gy.ka^{-1}).

Figure 3 displays single-grain OSL data in the form of the natural test dose response (which measures the sensitivity of a grain) as a function of the equivalent dose, for all selected grains. The effect of various grain selection criteria was extensively studied for the La Ferrassie samples by Guérin et al. (2015); as a consequence, we kept all grains for which the uncertainty on the test dose signal was smaller than 15%. For comparison with the study of Guérin et al. (2015), we first analyzed the single-grain OSL data using the Analyst software (Duller, 2015). The dose response curves were fitted with functions of the form:

$$\frac{L}{T} = a\,(1 - \exp(\frac{D}{D_c})),$$

where $\frac{L}{T}$ is the sensitivity-normalized OSL signal, a is the asymptotic limit, D is the radiation dose and D_c is the curvature parameter. For consistency with Guérin et al. (2015), we first estimated D_e values for only the grains whose curvature parameter (D_c in the equation above, D_0 in Guérin et al., 2015) value is greater than 100 Gy, as suggested by

Figure 2. Block of sediment associated with La Ferrassie 1 and still consolidated. Top: the dashed line indicates where we cut the block in two. Bottom: the part behind the bone sticking out was covered with plaster and used for OSL dating.

Thomsen et al. (2016) and Singh et al. (2017). The effect of such a selection criterion is to avoid biasing the distributions towards lower D_e values. In Figure 3, only those grains for which D_c>100 Gy are shown.

To estimate the variability in D_e values, we used the central dose model (CDM, Galbraith et al., 1999). For a first age estimate, instead of using the average of individual D_e values as in Guérin et al. (2015), we applied the Average Dose Model (ADM, Guérin et al., 2017). The main advantage of the ADM is that it appears to provide more accurate burial dose estimates than the CDM (which systematically underestimates). In addition, its burial dose estimates should be rather close to dose estimates calculated by Guérin et al. (2015) using an unweighted arithmetic average of D_e values.

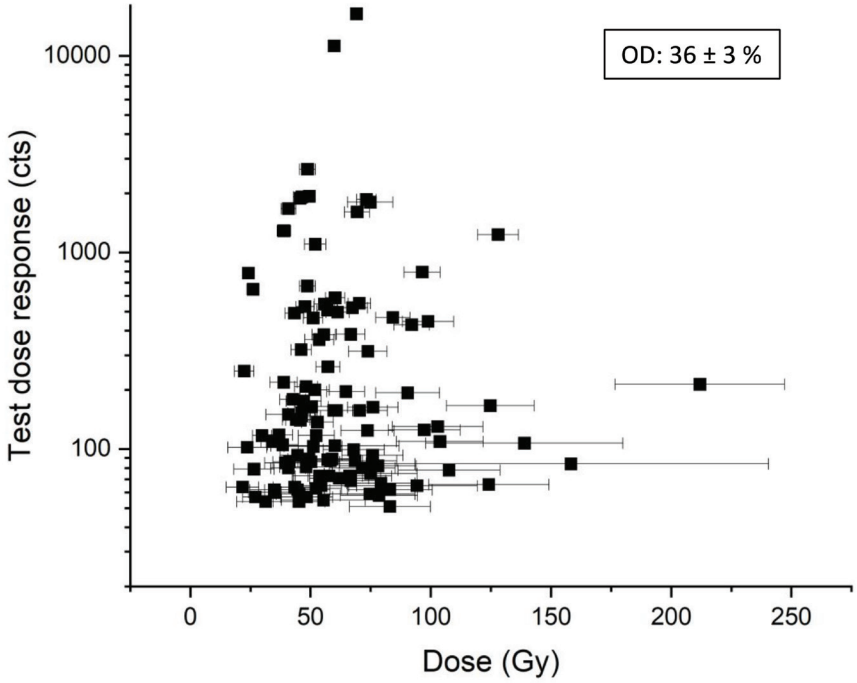

Figure 3. Test dose responses as a function of equivalent doses for the sample associated with La Ferrassie 1. For this plot, only the grains for which the curvature parameter (D_c) of the dose response curve were selected, among the grains that gave an uncertainty on the first test dose response smaller than 15%.

BAYESIAN MODELLING USING BAYLUM AND ARCHAEOPHASES

Generally, luminescence ages are calculated one at a time, sequentially through a series of calculations of equivalent doses for each measured aliquot, then of the central dose (or minimum dose) of these values, and of the average dose rate relevant to each sample. In this multi-step process, information is lost (see Combès et al., 2015), especially for samples where the natural OSL signal interpolates on the non-linear part of OSL dose response curve, close to saturation (e.g., Singh et al., 2017). In contrast, it is common practice that radiocarbon ages are calibrated and included in Bayesian models including stratigraphic constraints, with the aim to establish chronologies for stratigraphic sequences (Ramsey, 2009). In doing so, one makes use of available information on the ordering of ages to achieve better chronological resolution. While OxCal was specifically designed for modelling of radiocarbon ages, it is becoming increasingly common to also incorporate ages obtained using OSL and other methods (Douka et al., 2014; Frouin et al., 2017). However, an OSL age can only be included in OxCal in the form of a gaussian probability distribution, where all the uncertainty is treated as random. This mathematical description is quite problematic for OSL on several accounts, but in particular because a large fraction—typically most—of the errors affecting OSL ages come from systematic sources of errors (see, e.g., Murray et al., 2021). As a result, we decided not to model OSL ages using OxCal.

An alternative to OxCal modelling is provided by the open-source R package BayLum (Philippe et al., 2019; Christophe et al., 2020), specifically designed for OSL-based chronologies. BayLum uses raw OSL measurements to model dose distributions for series of OSL samples, but also allows modelling of the covariance in ages measured with the same equipment calibrated with the same standards (Guérin et al., 2021). Stratigraphic constraints may also be included, as well as radiocarbon ages—which are calibrated using IntCal20 (Reimer et al., 2020). By design, BayLum avoids the stepped data processing described in the previous paragraph; thus, the statistical inference using this tool is more consistent with the measured data. In addition, BayLum has already been shown in the literature to provide more accurate and precise ages based on laboratory experiments (Heydari and Guérin, 2018) as well as on dating studies of archaeological sites (Chevrier et al., 2020; Heydari et al., 2020; 2021; Guérin et al., 2022).

In the present study, three sets of samples from La Ferrassie are considered without established stratigraphic relationships between these sets: (i) the main sequence, already dated by Guérin et al. (2015) and Talamo et al. (2020) using OSL and radiocarbon (it is from Layer 5 of this main sequence that LF2 most likely comes); (ii) the area where LF8 was found (Balzeau et al., 2020, and references therein); and, (iii) the isolated sediment sample associated with LF1 dated here. While the samples from the latter two areas are chronologically unconstrained from a stratigraphic point of view, the main sequence comprises nine archaeological layers, which we used to impose stratigraphic constraints. That being said, the covariance of all OSL ages in the age calculations using BayLum, together with the stratigraphic

constraints and the independent, more precise ages such as those obtained with radiocarbon, are expected to increase the precision of the modelled chronology.

The input of BayLum consists of OSL measurements and dose rates to sedimentary grains, uncalibrated radiocarbon ages, stratigraphic constraints, and a matrix to account for systematic sources of errors. The matrix specifies not only individual uncertainties arising from unknown errors on laboratory beta dose rates, environmental beta, gamma and internal dose rates (0.06±0.03 $Gy.ka^{-1}$ following Mejdahl, personal communication to Murray, based on Mejdahl, 1987), but also the part of the variance that is shared across samples measured with the same equipment (Guérin et al., 2021). Ages and their probability densities are estimated jointly in BayLum through Markov Chain Monte Carlo (MCMC) calculations, which means that if the OSL age of one sample is constrained by independent ages—here radiocarbon ages—then all other OSL ages will also be constrained by the shared errors across OSL samples. In the present study, the errors that we consider systematic are those affecting: (i) the laboratory beta source calibration, (ii) the concentrations in K, U, and Th used as standards for the calibration of the gamma spectrometer, (iii) the *in situ* gamma dose rate measurements, and (iv) the internal dose rate to quartz grains.

To estimate phases—their start, end, duration, time range, etc.—we used the open-source R package ArchaeoPhases (Philippe and Vibet, 2020). This package contains a number of statistical tools to estimate parameters related to sequences of ages known though a Monte Carlo Markov Chains (MCMC) sample from their joint posterior distribution, thus representing probability density distributions of ages. Such samples may be provided by different chronological models, as for instance Baylum, Chronomodel (Lanos and Philippe, 2017; 2018) or Oxcal. ArchaeoPhases then performs post-treatment of the calculated ages; for example, one can specify a number of samples belonging to an archaeological layer and then estimate when the corresponding phase started, ended, how long it lasted, etc. Indeed, we have no direct dating for any of the skeletons included in the present study; for most of the studied skeletons, we have a set of ages from the layer where each skeleton was found. For LF1, we only have one OSL sample. Therefore, our aim is to compare the OSL age of this sample with the time ranges obtained for the layers of LF2 and LF8.

RADIOCARBON CALIBRATION: FROM INTCAL13 TO INTCAL20

Since Talamo et al. (2020) published their radiocarbon-based chronology for the main sequence using IntCal13 as the calibration curve, a new calibration curve was published—IntCal20 (Reimer et al., 2020). As a result, we have recalculated all radiocarbon ages using model 2 of Talamo et al. (2020), i.e., keeping the same modelling assumptions, stratigraphic constraints, etc.

In particular, for comparison with previously published data and interpretation, we kept the same modelling choices as those made by Talamo et al. (2020) when it comes to separating phases or archaeological layers. Between two successive layers (for example, when a gap between two successive layers was identified based on field observations), Talamo et al. (2020) sometimes used an extra boundary to distinguish the end of the lower layer from the start of the upper one (between Layers 6 and 7, and between Layers 7 and 8). In other places, where gaps between successive layers could not be identified, they merged these two events in one unique transitional boundary, i.e., a 'transition layer', defining both the end of the lower layer and the start of the upper layer.

Figures 4 and 5 show the updated radiocarbon chronology for the main archaeological sequence and for the remains associated with the LF8 individual.

RESULTS

FIRST AGE ESTIMATIONS FOR LA FERRASSIE 1

For the OSL sample associated with LF1, the radioelement concentrations are as follows: 0.90±0.02% of K, 2.8±0.2 ppm of U and 8.3±0.4 ppm of Th; all these values are in the range of concentrations measured for the previously studied samples from La Ferrassie (Guérin et al., 2015; Balzeau et al., 2020). The total dose rate to quartz grains is equal to 1.6±0.2 $Gy.ka^{-1}$.

The burial dose was determined using single-grain OSL measurements. A total of 3,500 grains were measured of which 252 gave a natural test dose uncertainty smaller than 15%; of these, 21 grains (8%) gave unbounded dose estimates using the Analyst software (Duller, 2015). 117 out of the 252 initially selected grains have a D_c value greater than 100 Gy and none of these 117 grains is close to saturation. For age calculation, we used these 117 grains for which the natural test dose uncertainty is smaller than 15% and D_c>100 Gy. The overdispersion (OD) value calculated for this population with the CDM is 36±3%. This value falls in the range of previously observed values for well-bleached samples from the site (which lie between 29% and 39%) and is significantly smaller than the OD value observed for poorly-bleached sample FER 2 (51±5%), which comes from the same area as the sample associated with LF1. The Average Dose Model (ADM: Guérin et al., 2017) gives a burial dose equal to 62±3 Gy and an age of 39±5 ka. Given the association with a Neanderthal skeleton, this age most likely corresponds to the end of the Middle Paleolithic and relates to Marine Isotope Stage (MIS) 3; it is statistically indistinguishable from the ages obtained for LF2, which most likely lies between 47 ka and 40±2 according to Guérin et al. (2015)—or between 54±4 and 40±2 ka if we include the possibility that LF2 was found in Layer 4—and between 49 and 44 ka (95% C.I.) according to Talamo et al. (2020). To compare this age with that determined for LF8, we are faced with an alternative—we may consider that the Neanderthal fragment, identified by aDNA among the remains associated to LF8 and which was dated to between 41.7 and 40.8 ka cal BP (95%), (i) belongs to LF8 and (ii) was not affected by contamination (see, e.g., Devièse et al., 2021). An

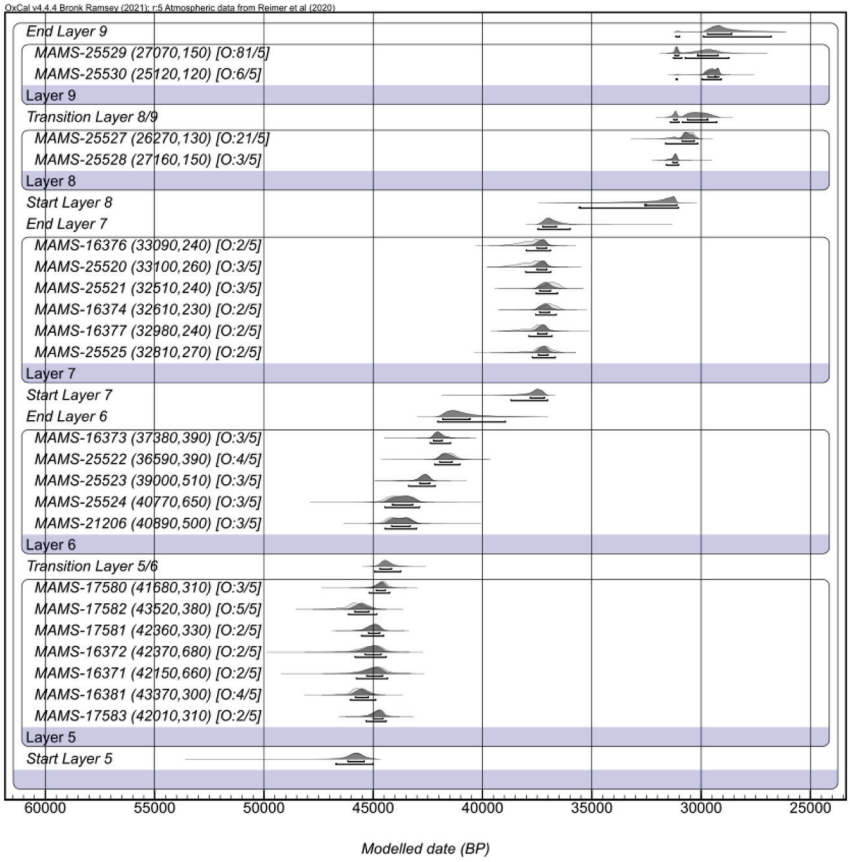

Figure 4. Oxcal modelling of the main archaeological sequence using IntCal20 (Reimer et al., 2020).

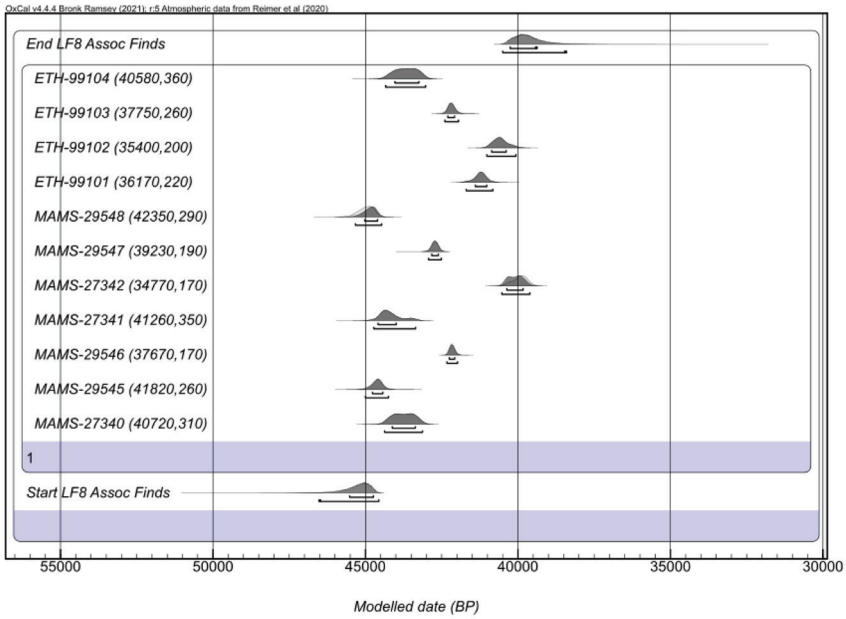

Figure 5. Oxcal modelling of the radiocarbon-based chronology for the remains associated with the La Ferrassie 8 individual.

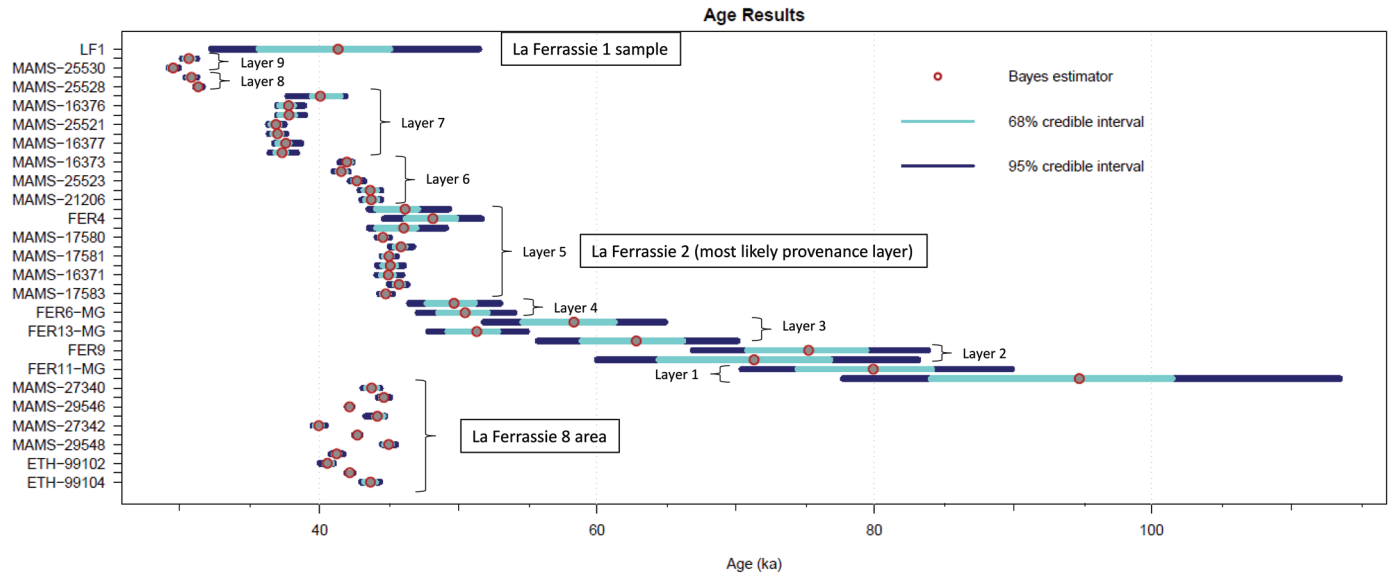

Figure 6. Ages calculated with BayLum with stratigraphic constraints and the θ matrix to account for systematic errors. The layer numbers correspond to the stratigraphy of the main sequence (Guérin et al., 2015). It should be noted here that one cannot exclude that the La Ferrassie 2 individual belonged to Layer 4. In any case, the ages obtained for each skeleton overlap at ~45 ka.

alternative possibility is to consider the age range obtained with radiocarbon on all the finds associated with LF8 as a more cautious time range (between 49.1–43.3 and 44.2–42.5 ka cal BP at 95% credibility level: Balzeau et al., 2020). In both cases, the LF1 age is compatible with that of LF8.

BAYESIAN INFERENCE USING BAYLUM

Figure 6 presents all ages calculated with BayLum, using stratigraphic constraints and a θ matrix to account for systematic errors. In the present case, systematic errors include components for calibration of the laboratory beta source dose rate, K, U, and Th concentrations of the standards used for calibration of the high-resolution gamma spectrometer, calibration of Al_2O_3:C dosimeters for *in situ* gamma dose rate measurements and the internal dose rate to quartz. It should be noted here that, since BayLum is insensitive to grain selection based on the curvature parameter (D_c) of the dose response curve (Heydari and Guérin, 2018), we included all grains from the LF1 sample for which the test dose uncertainty is smaller than 15% (n=252 grains). For our BayLum model, we specified a Gaussian dose distribution. 4.75 million iterations were required (counting adaptation, burn-in, and sampling) of the Monte Carlo Markov Chain procedure to reach convergence, as determined using the Gelman and Rubin's diagnostic (upper credible interval <1.05).

DISCUSSION

BAYESIAN MODELS: COMPARISON BETWEEN OXCAL AND BAYLUM/ARCHAEOPHASES

Prior to discussing the results, it is important to realise the different practices with respect to expressing ages and chronologies. While calibrated radiocarbon ages are given in thousand years Before Present (ka BP, before 1950), OSL ages are generally reported in ka before sampling time (in our case, 2011-15). As a result, since BayLum was developed specifically for OSL dating, we use the latter convention.

Turning to the main archaeological sequence of La Ferrassie, two chronological models are now available—one based on radiocarbon only, produced with the OxCal software; and, one obtained with BayLum, including both OSL and radiocarbon measurements. Before exploring the discrepancies between the two chronological inferences, one should first carefully examine the differences in the mathematical models, but only after careful definition of our objectives. Let us first examine the target events we are aiming at, discuss the link between these aims and our chronological data, and finally assess the adequacy of existing modelling tools to answer our questions.

Research Objectives and Modelling Tools

Our main research objective is to calculate the age of three of the Neanderthal skeletons found at La Ferrassie and, in particular, determine if they might have been contemporaries. Contemporaneity could, for instance, be discussed by DNA analyses, as in the case of the identification of the genome of the offspring of a Neanderthal mother and a Denisovan father (Slon et al., 2018) or of a Neanderthal father and daughter (Skov et al., 2022). Since such data are not available here, direct radiocarbon dating of the skeletons themselves appears to be the second-best option, but data are not at hand (unless the Neanderthal remain dated by Balzeau et al. (2020) belongs to LF8). The situation is made even less ideal by the fact that these skeletons were unearthed more than 50 years ago, and we are instead left with a number of OSL and radiocarbon ages associated

with the skeletons. Therefore, we need to make the following assumptions:

- the OSL age of the sediment associated with LF1 is representative of the age of the skeleton (no associated radiocarbon age exists for this skeleton);
- the ages of LF2 and LF8 can be determined using ages from the contexts (i.e., the respective archaeological layers) in which they were found. For LF2, this is most likely Layer 5, although one cannot confidently exclude Layer 4 (Guérin et al., 2015). For LF8, this phase is defined by all the finds labelled 'associated with the child' by its discoverer, H. Delporte. The underlying assumption is that we have enough data to characterize the chronological range of these archaeological assemblages, or, to put it differently, that the age of each skeleton does not lie outside our age sets. Having obtained 10 ages for Layer 5 and 11 for the LF8 area, we consider that this assumption is reasonable. In practice, we will consider that each of these two skeletons is an undated sample within its layer of provenance (note: an alternative for LF8 is to simply consider the dated Neanderthal remain from Balzeau et al., 2020).

As a result, we are interested in the chronological ranges of Layer 5 (or of Layers 4 and 5) inside the main sequence and of the assemblage associated with LF8, in comparison with the OSL age of the sediment associated with LF1.

In light of these considerations, OxCal allows the estimation of the beginning and end of phases (Ramsey, 2009). Using the function Date inside a phase set between two boundaries, Talamo et al. (2020) calculated the probable age of an undated sample inside this phase. Mathematically, this function starts with a prior uniform density distribution, within the interval defined by the phase boundaries, i.e., one assumes that the age of the undated sample (in our case, that of a skeleton) has equal probabilities of having an age anywhere inside the interval. As a result, the function Date exactly corresponds to our aim for the LF2 and LF8 individuals.

In comparison, the ArchaeoPhases package also allows estimation of the beginning and end of a phase. Likewise, it is possible (using the function undated_sample of ArchaeoPhases, version 1.8 and later: Philippe and Vibet [2020]) to estimate the age of a sample that would belong to a given phase (it is equivalent to the function Date of OxCal). The latter approach was already implemented on BayLum age calculations by Guérin et al. (2021). Here also, this latter function provides a result as close as possible to our target age within a layer. In addition, ArchaeoPhases includes the function PhaseTimeRange, which calculates, for a given credibility level, the interval inside which all ages of a phase are comprised.

In the following, we will compare, for each layer: (i) the estimates obtained by Oxcal and BayLum/ArchaeoPhases for the beginning and end of phases when only using radiocarbon ages; (ii) the outcome of the functions Date of Oxcal and undated_sample of ArchaeoPhases on the output of BayLum, still when using only radiocarbon ages; and, finally, (iii) the effect of including OSL data in the BayLum model before post-treatment with ArchaeoPhases.

But prior to these comparisons, we should first discuss the fundamental differences in modelling approaches, in order to understand and interpret potential differences.

Theoretical Considerations

First, we should discuss why OSL ages are not included in the OxCal model. In principle, it is possible to include OSL ages in OxCal models; however, then OSL ages are treated as gaussian distributions independent of each other. In particular, all the uncertainty assigned to each OSL age is treated as random. This is problematic because a large fraction of the OSL age uncertainties comes from the calibration of the equipment used in OSL dating. Calibration quartz (Hansen et al., 2015) used for laboratory beta source calibrations comes with an uncertainty corresponding to a systematic error affecting all doses delivered with the OSL readers calibrated with this reference quartz. Similarly, the calibration standards used for high-resolution gamma spectrometry measurements are only known to approximately ±2%. In total, a relative uncertainty of ~4–5% on each OSL age comes from such systematic errors. In favorable cases (i.e., when counting and other sources of random errors are minimal), most of the uncertainty on an OSL age actually comes from such systematic errors. Therefore, treating all uncertainty as random—as is done with OxCal—is unsatisfactory for OSL ages from first principles. In addition, including OSL ages in OxCal would require that these ages have been derived using a dose model such as the ADM after several steps of analysis during which information is increasingly lost. Thus, in our opinion modelling OSL ages with OxCal is not desirable.

When it comes to calibrating radiocarbon ages, BayLum uses a similar algorithm to that implemented in OxCal. Actually, comparisons of individual age calibration have led to indistinguishable calibrated ages (Guérin et al., 2022).

Besides those data that may or may not be satisfactorily included in OxCal and BayLum models, the main difference between these models lies in the definition and implementation of phases. OxCal, in general and at least as it was implemented by Talamo et al. (2020), uses the stratigraphic phasing as input of the model; it means that the defined phases influence the modelled ages. Conversely, in BayLum the phase definitions are not included in the age calculation and can thus not influence it. It is only after age calculation that ArchaeoPhases is used to estimate of phase parameters—just like the un_dated function of Oxcal comes after age calculation. Mathematically, in OxCal the posterior density of a set of r ages defining a phase with a start α and end β is proportional to $\frac{1}{(\alpha-\beta)}$ (Ramsey, 2009). As a consequence, the OxCal model of a phase tends to favor shorter durations, since the posterior probability density becomes larger when the interval between α and β decreases, leading to a 'concentration effect' as demonstrated by Lanos and Philippe (2018). This being said, in OxCal by definition the phase boundaries may extend outside the interval defined by the youngest and oldest individual ages

inside the phase (NB: here one excludes from the discussion cases where outliers are detected), because for every r then $\alpha<a_r<\beta$, where a_r is the age of sample r. By contrast, in ArchaeoPhases the beginning of a phase corresponds to the oldest age from this phase and its end to the youngest age.

From first principles, it is very difficult to decide which modelling approach is most appropriate. To complicate things further, it seems difficult to empirically test which model better characterizes known phases, because such phases are generally unknown. While assessing the validity of a dating method generally relies on comparing obtained ages with independent, well-established methods (e.g., Murray and Olley, 2002; Buylaert et al., 2009; 2012), then the phase duration is generally not testable using other methods. As a result, we cannot easily decide which of the two modelling approaches is most appropriate. In the absence of reference data, a solution to discuss the validity of statistical models is to compare the inferences drawn from the data with the data themselves. *A priori*, we can say that the combination of BayLum and ArchaeoPhases appears to stick more to the measured data than OxCal, which (i) includes the phases definition in age calculation, and (ii) calculates phase boundaries (α,β) outside the calculated age range. In the following, we discuss the different phase estimates obtained from the two modelling solutions in the light of measured (and, in the case of radiocarbon, calibrated) ages, in an attempt to identify which mathematical tool—if any—gives chronological inferences that fit the experimental observations better. In other words, we define the consistency of each model by comparison of its inferences with calibrated ages; if the extent of a modelled phase differs from the individual ages measured inside this phase, then we consider that this inference is not supported by data.

As a final note, in both the OxCal and BayLum/Archaeophases approaches, modelling relies on the quantity and quality of the input data and we can reasonably assume that, if sampling is well suited to the chronological questions at stake, both solutions will converge towards the same scenario. Nevertheless, we should keep the fundamental modelling differences in mind when discussing the chronological inferences.

Comparison of Modelled Chronologies: OxCal vs BayLum/ArchaeoPhases

Table 2 lists, for each layer from 1 to 9 in the main excavation area, and for samples associated with LF8, the 95% C.I. for the start and end and of the corresponding phases using either (i) only radiocarbon ages modelled with OxCal, (ii) only radiocarbon ages modelled with BayLum/ArchaeoPhases, or (iii) radiocarbon and OSL ages modelled with BayLum/ArchaeoPhases. This table also gives the time range of each phase, i.e., the interval comprising all ages of the phase at the 95% credibility level. A first observation is that for each layer, the phase time range almost exactly corresponds to the interval defined by the upper limit (older age value) of the oldest age within the phase and the lower limit (younger age value) of the youngest age within the phase. In other words, the phase time range function of the ArchaeoPhases package is quite transparent and provides intuitive results; the end (respectively, the beginning) of a phase is defined by the youngest (respectively, oldest) sample inside this phase. As we will see below, OxCal sometimes provides very different results.

Since OxCal is a reference software while the open-source BayLum and ArchaeoPhases packages are still relatively new, in the following we compare the results obtained with the two approaches in detail, especially when only radiocarbon is used for building chronologies. Nevertheless, to give a quick overview of the situation, in Figure 7 we show individual radiocarbon ages (95% C.I.), as measured and calibrated independently of the sequence at stake, together with the phase boundaries (95% C.I.) estimated using these data by OxCal on the one hand and BayLum/ArchaeoPhases on the other. In Figure 8, individual radiocarbon ages are also plotted, but this time together with the 95% C.I. obtained for an undated sample inside each phase. From these figures, we observe that BayLum/ArchaeoPhases give estimates of the start, the end, and one undated sample for each phase that appear to be closer to the measured data than OxCal. This conclusion is examined in more detail for each layer below.

Layer 9. Only two radiocarbon (and no OSL) samples were dated from Layer 9, giving the two following 95% C.I. after calibration using OxCal and IntCal20: [29.9; 29.2] and [31.5; 31.0] ka. It should be noted that here and in the following discussion, unless explicitly mentioned otherwise, we report the calibrated ages as calculated without the chronological model of the sequence, i.e., they correspond to the measured ages after calibration. When using only radiocarbon for the chronological models, BayLum/ArchaeoPhases give, for the start of this period, the interval [31.3; 30.0] ka, while OxCal gives [31.5; 29.3]. As far as the end of the layer is concerned, BayLum/ArchaeoPhase gives [29.8; 29.1] ka, compared to [29.9; 26.9] ka (OxCal). It seems clear that OxCal extends the phase boundaries quite far away from the measured (and calibrated) radiocarbon ages; this observation is especially true for the end of the phase, which may extend to 26.9 according to OxCal, whereas no individual age extends further than 29.2 ka at the 95% credibility level. In other words, the chronological model implemented in OxCal considers it quite likely that the phase corresponding to layer 9 did extend in time more than 2,000 years after the most recent dated sample. Unsurprisingly, the inclusion of OSL ages in the BayLum/ArchaeoPhases model barely affects the age estimates for the start and end of the period.

Finally, the 95% C.I. for the age of an undated sample from Layer 9 differs quite significantly between OxCal and BayLum/ArchaeoPhases giving [30.2; 28.2] and [31.2; 29.4] ka, respectively.

Layer 8. From Layer 8, only two samples were dated (both radiocarbon samples). When calibrated independently of the sequence, they gave the following 95% C.I.: [31.6; 31.1] ka and [31.0; 30.2] ka, respectively. When using only radiocarbon as input, BayLum/ArchaeoPhases gives, for

TABLE 2. NINETY-FIVE % CREDIBLE INTERVALS FOR THE START, END, AND AN UNDATED SAMPLE INSIDE OF EACH LAYER, ESTIMATED EITHER WITH (I) OXCAL USING ONLY RADIOCARBON, (II) BAYLUM AND ARCHAEOPHASES USING ONLY RADIOCARBON, AND (III) BAYLUM AND ARCHAEOPHASES USING RADIOCARBON AND OSL AGES.

	Oxcal, radiocarbon only*			BayLum/ArchaeoPhases, radiocarbon only*				BayLum/ArchaeoPhases, radiocarbon and OSL*			
Phase	**Start**	**End**	**Undated sample**	**Start**	**End**	**Undated sample**	**Phase Time Range**	**Start**	**End**	**Undated sample**	**Phase Time Range**
Layer 9	31.5; 29.3	29.9; 26.9	30.2; 28.2	31.3; 31.0	29.8; 29.1	31.2; 29.4	31.3; 29.2	**31.1; 30.1**	**29.8; 29.1**	**30.7; 29.2**	**31.1; 29.1**
Layer 8	36.0; 31.1	31.5; 29.3	34.1; 29.6	31.6; 31.1	30.9; 30.2	31.4; 30.4	31.6; 30.2	**31.6; 31.1**	**31.1; 30.4**	**31.4; 30.6**	**31.6; 30.4**
Layer 7	39.4; 37.2	37.6; 36.1	38.6; 36.5	39.1; 37.4	37.1; 36.2	38.5; 36.5	39.1; 36.3	**41.7; 38.2**	**37.1; 36.3**	**40.7; 36.5**	**41.6; 36.2**
Layer 6	45.0; 43.7	42.1; 38.5	44.7; 40.2	44.7; 43.5	42.0; 41.0	44.5; 40.9	44.5; 41.0	**44.5; 43.3**	**42.0; 41.0**	**44.1; 41.4**	**44.5; 41.0**
Layer 5	46.7; 45.0	45.0; 43.7	46.1; 44.2	46.8; 45.4	44.8; 44.1	46.2; 44.4	46.8; 44.0	**51.6; 45.7**	**44.8; 43.7**	**49.6; 44.1**	**51.6; 43.4**
Layer 4								**54.3; 47.4**	**52.9; 46.5**	**53.5; 46.9**	**54.1; 46.4**
Layer 3								**70.4; 56.7**	**55.1; 47.9**	**65.7; 49.9**	**70.0; 47.7**
Layer 2								**85.6; 68.1**	**80;7; 60.1**	**83.1; 64.0**	**85.6; 60.5**
Layer 1								**113.7; 78.9**	**90.0; 70.8**	**103.2; 74.2**	**113.1; 69.8**
LF8	46.6; 44.6	40.6; 38.4	45.6; 39.5	45.5; 44.5	40.4; 39.5	44.9; 39.9	45.5; 39.5	**45.5; 44.6**	**40.4; 39.5**	**45.5; 39.5**	**45.5; 39.5**

*The ages are given in thousand years (ka) before 2011 (sampling year; thus, they correspond to radiocarbon calibrated ages, except that the reference for radiocarbon is 1950 whereas we took 2011, i.e. the OSL sampling year, as our t_0). For the BayLum/ArchaeoPhases models, the 95% C.I. containing all ages is also given. Our best estimates are given in bold (see text for details).

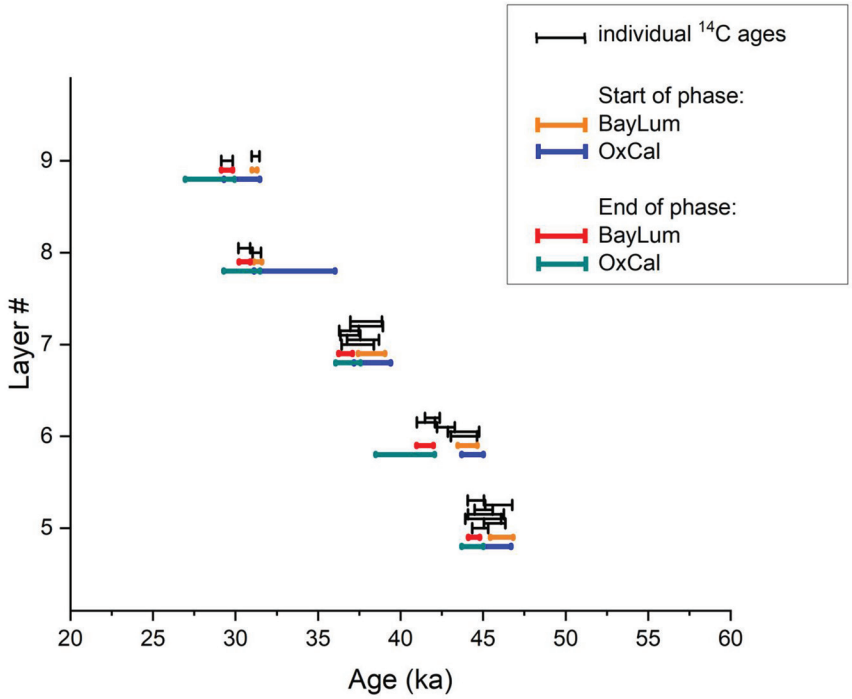

Figure 7. Comparison between OxCal and BayLum/ArchaeoPhases models, when using only radiocarbon as input data: phase starts and ends. All intervals correspond to the 95% credibility level: individual radiocarbon ages calibrated independently (thin black bars); phase starts (orange thick bars) and ends (red thick bars) estimated with BayLum/ArchaeoPhases; phase starts (blue thick bars) and ends (cyan thick bars) estimated with OxCal.

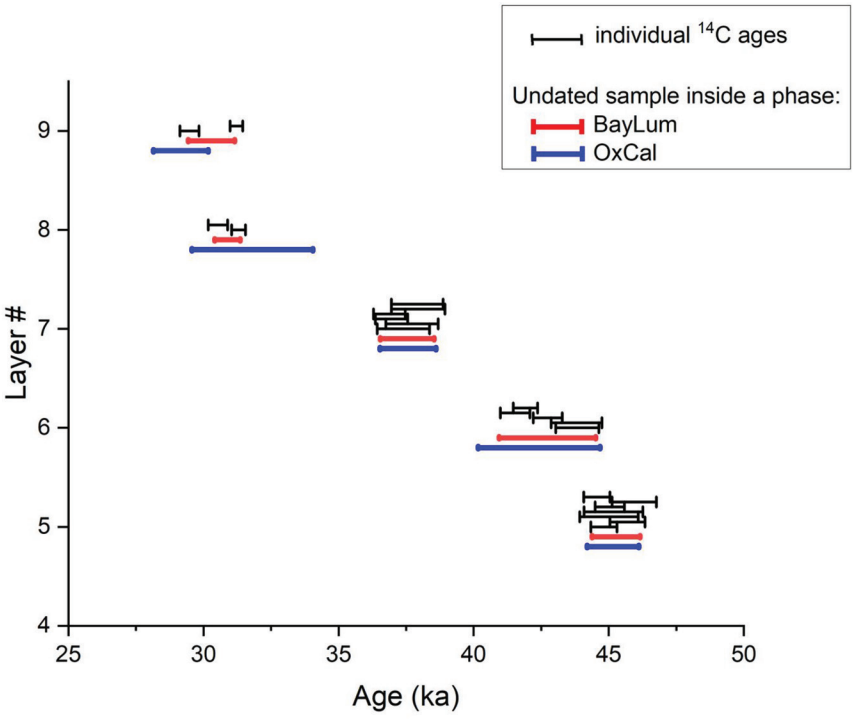

Figure 8. Comparison between OxCal and BayLum/ArchaeoPhases models, when using only radiocarbon as input data: undated sample within each phase. All intervals correspond to the 95% credibility level: individual radiocarbon ages calibrated independently (thin black bars); undated samples estimated with BayLum/ArchaeoPhases (red thick bars); and, with OxCal (blue thick bars).

the start of this period, the interval [31.6; 31.1] ka, while Oxcal gives [36.0; 31.1] ka. It is here very clear that BayLum/ArchaeoPhases takes the oldest sample as the marker of the end of the phase, while OxCal extends the start of the phase up to 36.0 ka, which is several thousand years earlier than the youngest dated sample from Layer 8. As stated above, we have no way of knowing when this phase started, so we cannot prove any given model to be in error; all we can say is that BayLum/ArchaeoPhases, contrary to Oxcal, does not extrapolate the phase beyond measured ages.

Regarding now the end of Layer 8, BayLum/ArchaeoPhases gives the interval [30.9; 30.4] ka, while Oxcal gives [31.5; 29.3]. Here again, the lower end of the interval given by BayLum/ArchaeoPhases (30.2 ka) matches the lower end of the youngest calibrated age 95% C.I. (30.2 ka), contrary to that given by Oxcal (29.3 ka). The latter is actually very close to the older end of the youngest calibrated age from Layer 9 above (29.2 ka), which is somewhat surprising. Here again, as for the start of this phase, BayLum/ArchaeoPhases appears to give estimates closer to the measured data.

As expected for this layer, the inclusion of OSL ages in BayLum/ArchaeoPhases only marginally affects the statistical inference. Finally, the age of an undated sample from Layer 8 very strongly depends on the modelling choice between OxCal: [34.1; 29.6] ka and BayLum/ArchaeoPhases: [31.4; 30.4] ka. Not only is the latter much more precise but it also fits more closely with the observed ages.

Layer 7. For this layer, six radiocarbon and one OSL (39.9±2.5 ka) ages are available. Putting the OSL sample aside for a moment, the 95% C.I. phase time range for this layer is [39.1; 36.3] ka, which means that all six radiocarbon ages retained for this study are clustered inside this interval. According to BayLum/ArchaeoPhases, the start of this layer lies somewhere in the interval [39.1; 37.4] ka and it ends in the interval [37.1; 36.2] ka. OxCal gives very similar ranges, i.e. [39.4; 37.2] ka for the start and [37.6; 36.1] ka for the end. The age of an undated sample from Layer 7 determined with BayLum/ArchaeoPhases is [38.5; 36.5] ka and is very similar to that determined with OxCal—[38.6; 36.5] ka.

For this layer, the most notable difference in chronological inference comes when including the OSL sample FER1—while the C.I. for the end ([37.1; 36.3] ka) is essentially unchanged, the C.I.s for the start and the age of an undated sample move towards older ages: [41.7; 38.2] and [40.7; 36.5] ka, respectively. This is not surprising because this OSL sample appears to be, in the BayLum/ArchaeoPhases model, the oldest sample from this layer (see Figure 5).

But then how can we interpret this change in the estimation of the start and range of this layer? A first observation in passing is that, if we were to include all radiocarbon ages measured by Talamo et al. (2020) and thus include three samples considered as outliers from this layer (Layer 7), the phase time range determined with BayLum/ArchaeoPhases with only radiocarbon (n=9) would become [40.9; 36.2] ka. This is actually very close to the phase time range determined with only six radiocarbon samples and the OSL one. In other words, this observation might suggest that the three radiocarbon samples considered to be outliers could actually reflect a rather long duration of the occupations from Layer 7 (note: Sample MAMS-17584, field code L5-204, is incorrectly attributed to Layer 7 in Figure 3A of Talamo et al. [2020] and in their subsequent analysis. Its correct attribution is Layer 6. However, the results remain unchanged as this sample was disregarded because of its context next to the cave wall where movement and contamination was possible. Excluding this sample from Layer 7 here gives a time range equal to [39.5; 36.2] ka, which remains significantly shorter than the interval determined when including the OSL age for this layer.)

More generally, the next question is the time lapse represented by the archaeological layers—in particular, here Layer 7—in comparison with the resolution of the implemented dating methods. This question is all the more complex because the resolution of radiocarbon and OSL are quite different—radiocarbon being more precise than OSL. Unfortunately, it is very difficult, with the present state of the methods, to know how much time an archaeological layer represents, so we are forced to make guesses.

In a first scenario, let us assume that the archaeological record corresponds to a period much shorter than all age uncertainties. One would then expect all ages to be consistent with at least one precise age—and one should remove too imprecise estimates, such as OSL ages. Indeed, the OSL age from this layer only contributes the information that the layer could have started earlier than predicted by radiocarbon.

In a second scenario, let us assume that the archaeological record corresponds to a period much longer than all age uncertainties. One would then expect data much more dispersed than the uncertainties; in the case of Layer 7, where nine samples were radiocarbon dated, this observation only holds true if we include samples believed to be outliers according to Talamo et al. (2020). In addition, the area of provenance of the radiocarbon samples is rather limited—especially since outliers were removed because they were supposedly affected by the wall effect. As a result, perhaps we are looking at a small fraction of the time of Layer 7 simply because we are looking at a small fraction of its extent, due to the limited size of the excavation area. In this second scenario, it may be that OSL rightfully represents an earlier part of the layer that was not captured by the radiocarbon sampling. In such a case, then it becomes useful to incorporate OSL in the chronological models.

We admittedly cannot test these assumptions—and the data do not really seem to us to clearly favor one assumption over the other. Therefore, for the following layers, we will keep the more cautious approach consisting of using both OSL and radiocarbon ages, at the risk of losing precision.

Layer 6. Only one OSL sample was measured from this layer and it turned out to be insufficiently bleached, i.e., it required minimum age modelling in order to derive an accurate burial age. However, since such a specific model-

ling tool is not available in BayLum, we exclude this OSL sample from our analysis. Thus, for this layer only five radiocarbon ages are available. Layer 6 is interesting because some individual age intervals from Layer 5 and 6 overlap, so the start of Layer 6 not only depends on the ages derived for Layer 6, but also on Layer 5 ages.

In this context, BayLum and ArchaeoPhases give [44.7; 43.5] ka for the start, [42.0; 41.0] for the end and [44.5; 41.0] for the range of this Chatelperronian layer (note: including all OSL ages in the sequence model does not make a significant difference with respect to Layer 6 estimates under study). According to OxCal, these intervals are [45.0; 43.7] ka and [42.1; 38.5] ka for the start and end, respectively. The main difference between the model outputs lies in the estimation of the end of the phase, which is not constrained by overlying ages. As already observed in particular for Layer 9, the end of the phase as estimated with OxCal extends to much younger times than individual ages suggest (the youngest dated sample from Layer 6 is [42.0; 40.5] ka at 95% credibility, so there are no data to suggest that Layer 6 could have lasted until 38.5 ka). We conclude that the statistical inference drawn by BayLum/ArchaeoPhases is more consistent with the measurements. Conversely, the start of Layer 6 is constrained by underlying ages from Layer 5: as a result, the estimates for the start of the phase depend very little on which model is used.

Layer 5. Layer 5 is the last layer for which radiocarbon ages are reliable, since all samples from Layer 4 appear to be outliers (Talamo et al., 2020) and one sample from Layer 3 gives an unbounded age interval because it is too close to the limit of the IntCal20 curve. As a result, in the present study we did not include radiocarbon ages below Layer 5.

Three OSL and seven radiocarbon samples were dated from Layer 5, which makes it the most extensively studied phase of the site (it is also the most likely provenance of LF2 and, by extension, LF1).

Leaving aside the OSL ages for a moment, BayLum and ArchaeoPhases give [46.8; 45.4] ka for the start, [44.8; 44.1] ka for the end and [46.8; 44.0] ka for the range of Layer 5. In comparison, with OxCal we obtain [46.7; 45.0] ka and [45.0; 43.7] ka for the start and end of Layer 5, respectively. For this layer, both modelling approaches give similar results for the start and end of the period; for the end, this is probably because the end of this layer is constrained by the beginning of Layer 6 above, just like the latter is constrained by Layer 5 ages (as discussed in the previous sub-section). For the start of the phase, however, one might have expected that OxCal would extend the 95% C.I. to older ages, as it extends beyond the range of the ages for Layers 9, 8, and 6 (only regarding the end of Layer 6; see Figure 7). A possible explanation is that enough ages are available for OxCal to estimate the start of the corresponding phase; this explanation would confirm our expectation that the more data are available, the less the chronological inference depends on the choice of modelling tool. In other words, for Layer 5 data—rather than modelling—drive our estimates.

If one includes OSL in the modelling, the estimate of the end of Layer 5 is essentially unchanged. However, the start of the phase extends to older ages, i.e., to [51.6; 45.7] ka at 95% credibility. This change is similar to that observed for Layer 7 when including OSL. Because of the larger age uncertainties attributed to OSL compared to radiocarbon, BayLum/ArchaeoPhases extends the possible duration of the phase. Whether this extension reflects a true longer duration of the phase or is the sole result of poor resolution of OSL dating compared to the time lapse under study remains, like for Layer 7, an open question at this stage. Cautiously, we retain the less precise interval—at least until one can demonstrate that occupations from Layer 5 did not last longer than several centuries.

As a result, using the function undated_sample of ArchaeoPhases applied to the BayLum model including all OSL and radiocarbon data for the sequence, we estimate an age of 49.6 to 44.1 ka for the LF 2 individual (95% credibility) if we assume it was found in Layer 5.

Bottom Part of the Main Sequence (Layers 4 to 1)

Since radiocarbon is more precise than OSL, it clearly has a dominant effect on the chronological inferences for Layers 9 to 5. However, from Layer 4 downwards, only OSL ages are available. As a result, we only modelled the bottom layers using BayLum/ArchaeoPhases and including OSL in the model.

Layer 4 clearly was deposited during MIS 3 and is very close in time, at least at the scale of the OSL resolution, to Layer 5. The corresponding phase time range is only shifted ~2,500–3,000 years (see Table 2); since we cannot exclude Layer 4 as the provenance of LF2 (and so LF1, by association), this is rather fortunate because the effect of this uncertainty on the age of the skeleton is rather limited. Using the function undated_sample of ArchaeoPhases on Layer 4, we can claim that LF2 cannot be older than 54.1 ka (with 95% credibility).

For Layers 1–3, our results remain very similar to those already reported by Guérin et al. (2015) and Frouin et al. (2017). If Layer 3 ended during MIS 3 (between 55.1 and 47.9 ka), we cannot state whether it started during MIS 4 or during the early MIS 3. The sediment from this layer does not show cold features such as ice lensing, but as Pederzani et al. (2021) showed at la Ferrassie, one should be cautious when relying on environmental proxies to determine the isotopic stage one is looking at.

Conversely, based on its age, Layer 2 most likely corresponds to MIS 4, which appears to be consistent with micromorphological features such as ice lenses observed in thin sections.

Finally, Layer 1 was deposited, at least in part, during MIS 5—most likely in totality.

La Ferrassie 8 Area

To estimate the chronology of LF8, only radiocarbon ages (n=11) are available and their individual ages (95% C.I.) all lie between 45.6 and 39.6 ka (note: these interval boundaries are within 0.1 ka of the phase time range given by ArchaeoPhases). As could be expected, regardless of whether OSL is included, the BayLum model does not change the statisti-

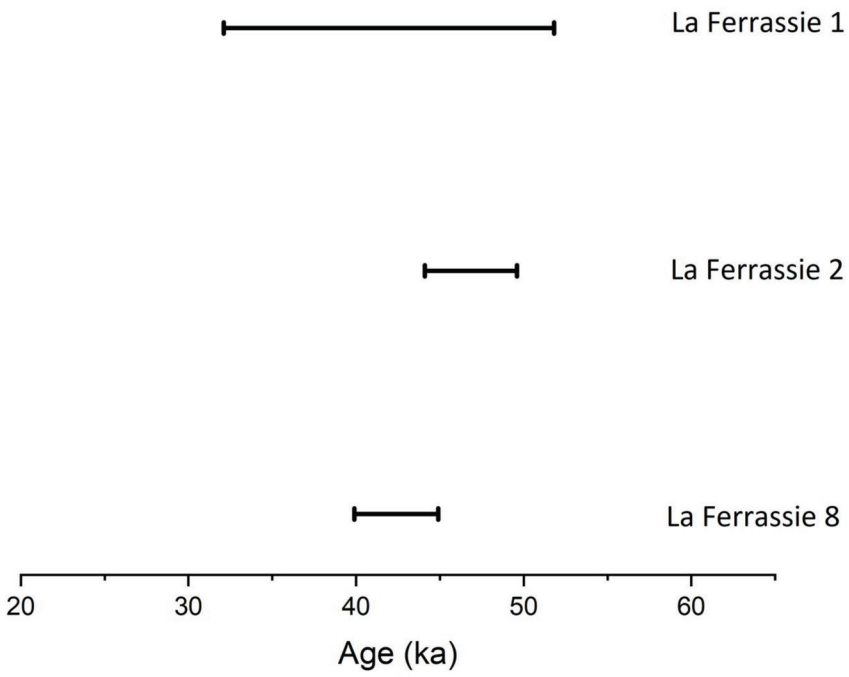

Figure 9. Ninety-five % credible intervals of our best estimates for the ages of the three skeletons La Ferrassie 1, 2, and 8 (see text for details). The three intervals overlap in the range [44.9; 44.1] ka.

cal inference. When comparing models, BayLum/ArchaeoPhases gives [45.5; 44.5] ka for the start compared to [46.6; 44.6] according to OxCal; clearly, BayLum/ArchaeoPhases is more consistent with the measured data. Similarly, for the end of the phase the interval given by OxCal ([40.6; 38.4] ka) extends outside the individual 95% C.I.s, contrary to BayLum/ArchaeoPhases ([40.4; 39.5] ka).

Assuming *a priori* that the age of LF8 can lie anywhere with equal probability inside the phase defined by all finds associated with it, the function undated_sample of ArchaeoPhases gives an age of [44.9; 39.9] ka (95% C.I.). Alternatively, LF8 is directly dated by the Neanderthal bone from Balzeau et al. (2020) and its age is between 41.7 and 40.8 ka (95% C.I.).

Overview of Modelling Approaches

Based on our systematic comparison of statistical inferences obtained with OxCal on the one hand and with BayLum/ArchaeoPhases on the other, we reach two conclusions:

- BayLum/ArchaeoPhases always gives more precise estimates of phase than OxCal; and
- the statistical inferences drawn with BayLum/ArchaeoPhases are always more consistent with the measurements than those drawn with OxCal.

Consequently, in the following we base our discussion of the results obtained with BayLum and ArchaeoPhases.

PALEOANTHROPOLOGICAL IMPLICATIONS: THE NEANDERTHALS FROM LA FERRASSIE

The best age estimates for all three individuals (i.e., LF1: [32.1; 51.8] ka, LF2: most likely [49.6; 44.1] ka, but [53.5; 46.9] ka cannot be excluded, and LF8: [44.9; 39.9] ka with certainty, possibly [41.7; 40.8] ka) place them in the middle of MIS 3. Figure 9 shows these 95% credibility time intervals for the three skeletons (assuming for LF2 that it belongs to Layer 5 rather than to Layer 4). The three intervals overlap in the range [44.9; 44.1] ka, which means that these three Neanderthal individuals could have been at least broadly contemporary.

This statement leads us to make a few additional remarks. First, the current resolution of our dating methods prevents us from being more specific. It seems that only genetic analyses might answer the question of contemporaneity of the skeletons. Direct dating of the human remains from these three skeletons using radiocarbon would certainly give more precise age estimates (e.g., Talamo et al., 2016; Balzeau et al. 2020; Hublin et al., 2020), but would not answer the question of contemporaneity because of uncertainties that would be too large.

Second, one should also comment on the apparent dispersion in radiocarbon ages from the LF8 sector. In the light of the burial hypothesis formulated by Balzeau et al. (2020), if LF8 was indeed buried, then logically the age of the skeleton would be the youngest dated sample from this area ([40.5; 39.6] ka at the 95% credibility level), because once it was buried no younger elements could have come in association with the skeleton. One may note here that the human remain dated by Balzeau et al. (2020) is not the most recent radiocarbon age in the series. While outliers appear rather frequently in the radiocarbon literature, the fact that stratigraphy is poorly constrained for the LF8 remains might explain why no outlier was identified. It may also be that all radiocarbon ages from this sample set are both precise and accurate.

As frustrating as these remarks may be, they must be born in mind when discussing the age of the skeletons.

CONCLUSION

This study builds upon 46 ages (33 radiocarbon and 13 OSL) combined in a Bayesian chronological model using a relatively new tool—the open-source software package BayLum. When considering radiocarbon only, the combination of BayLum and ArchaeoPhases is shown to provide chronological inferences that are more precise and more consistent with the measured data than the widely-used OxCal software. In addition, BayLum allows the inclusion of OSL ages in a manner that reflects the specificities of OSL dating, in particular systematic errors.

Based on these measurements, modelling and contextual information, at least three of the seven Neanderthal skeletons found at La Ferrassie date from the end of the Middle Paleolithic (LF1, LF2, and LF8) and are all younger than 52 ka, at the 95% credibility level. In particular, the age estimated for LF1 lies between 32 and 52 ka (95% C.I.). These three individuals might even have been contemporaries, in which case their age would be constrained between 44.9 and 44.1 ka based on our measurements and a set of hypotheses regarding their original context. However, if the Neanderthal remain directly dated by radiocarbon in Balzeau et al. (2020) actually belongs to LF8, then this individual is more recent than LF2. In such a case, LF1 might have been contemporary with either LF2 or LF8.

As a final note, one may hope that direct dating of human remains from La Ferrassie will someday improve our knowledge of the chronology of these individuals. In any case, these ages place LF1, LF2, and LF8 among the latest Neanderthals in Europe and open important perspectives for the discussion on the disappearance of this humanity.

ACKNOWLEDGEMENTS

This article is part of the ERC QuinaWorld project (Starting Grant #851793 awarded to GG). Research at La Ferrassie was also funded by the Région Aquitaine through the NEMO, CHROQUI, and NATCH projects. AGO has received support from the Spanish Ministerio de Ciencia e Innovación (proyecto PGC2018-093925-B-C33, MCI/AEI/FEDER, UE), Research Group IT1418-19 from the Eusko Jaurlaritza-Gobierno Vasco, and by a Ramón y Cajal fellowship (RYC-2017-22558).

DATA STATEMENT

Data will be made available upon request.

REFERENCES

Balzeau, A., Turq, A., Talamo, S., Daujeard, C., Guérin, G., Welker, F., Crevecoeur, I., Fewlass, H., Hublin, J.-J., Lahaye, C., Maureille, B., Meyer, M., Schwab, C., Gómez-Olivencia, A., 2020. Pluridisciplinary evidence for burial for the La Ferrassie 8 Neandertal child. Sci. Rep.10, 21230.

Bøtter-Jensen, L., Bulur, E., Duler, G.A.T., Murray, A.S., 2000. Advances in luminescence instrument systems. Radia. Meas. 32, 523–528.

Buylaert, J.P., Murray, A.S., Thomsen, K.J., Jain, M., 2009. Testing the potential of an elevated temperature IRSL signal from K-feldspar. Radia. Meas. 44(5-6), 560–565.

Buylaert, J.-P., Jain, M., Murray, A.S., Thomsen, K.J., Thiel, C., Sohbati, R., 2012. A robust feldspar luminescence dating method for Middle and Late Pleistocene sediments." Boreas 41, 435–451.

Capitan, L., Peyrony, D., 1909. Deux squelettes humains au milieu de foyers de l'époque moustérienne. C.R. Séances Acad. Inscr. B.-Lett. 53(11), 797–806.

Capitan, L., Peyrony, D., 1912a. Station préhistorique de La Ferrassie, commune de Savignac-du-Bugue (Dordogne). Rev. Anthropol. 2, 76–99.

Capitan, L., Peyrony, D., 1912b. Trois nouveaux squelettes humains fossiles. C.R. Séances Acad. Inscr. B.-Lett. 56(6), 449–454.

Chevrier, B., Lespez, L., Lebrun, B., Garnier, A., Tribolo, C., Rasse, M., Guérin, G., Mercier, N., Camara, A., Ndiaye, M., Huysecom, E., 2020. New data on settlement and environment at the Pleistocene/Holocene boundary in Sudano-Sahelian West Africa: interdisciplinary investigation at Fatandi V, Eastern Senegal. PLoS One 15(12), e0243129.

Christophe, C., Philippe A., Kreutzer S., and G. Guerin, 2020. BayLum: chronological Bayesian models integrating optically stimulated luminescence and radiocarbon age dating. R package version 0.2.0. https://CRAN.R-project.org/package=BayLum

Combès, B., Philippe, A., 2017. Bayesian analysis of individual and systematic multiplicative errors for estimating ages with stratigraphic constraints in optically stimulated luminescence dating. Quatern. Geochronol. 39, 24–34.

Combès, B., Lanos, P., Philippe, A., Mercier, N., Tribolo, C., Guérin, G., Guibert, P., Lahaye, C., 2015. A Bayesian central equivalent dose model for optically stimulated luminescence dating. Quatern. Geochronol. 28, 62–70.

Delibrias, G., 1984. La datation par le carbone 14 des ossements de la Ferrassie. In: Delporte, H., Le Grand Abri de La Ferrassie. Éditions du Laboratoire de Paléontologie Humaine et de Préhistoire, Paris, pp. 105–107.

Delporte, H., 1984. Le Grand Abri de La Ferrassie. Éditions du Laboratoire de Paléontologie Humaine et de Préhistoire, Paris.

Delporte, H., Tuffreau, A., 1973. Les industries du Perigordien superieur de Ia Ferrassie. Quartär 23/24, 93–123.

Devièse, T., Abrams, G., Hajdinjak, M., Pirson, S., De Groote, I., Di Modica, K., Toussaint, M., Fischer, V., Comeskey, D., Spindler, L., Meyer, M., Semal, P., Higham, T., 2021. Reevaluating the timing of Neanderthal disappearance in Northwest Europe. Proc. Nat. Acad. Sci. 118(12), e2022466118.

Douka, K., Jacobs, Z., Lane, C., Grün, R., Farr, L., Hunt, C., Inglis, R.H., Reynolds, T., Albert, P., Aubert, M., Cullen, V., Hill, E., Kinsley, L., Roberts, R.G., Tomlinson, E.L., Wulf, S., Barker, G., 2014. The chronostratigraphy

of the Haua Fteah cave (Cyrenaica, northeast Libya). J. Hum. Evol. 66, 39–63.

Duller, G.A.T., 2015. The Analyst software package for luminescence data: overview and recent improvements. Ancient TL 33(1), 35–42.

Duller, G.A., Bøtter-Jensen, L., Murray, A.S., Truscott, A.J., 1999. Single grain laser luminescence (SGLL) measurements using a novel automated reader. Nucl. Instrum. Methods Phys. Res. B 155(4), 506–514.

Frouin, M., Lahaye, C., Valladas, H., Higham, T., Debénath, A., Delagnes, A., Mercier, N., 2017. Dating the Middle Paleolithic deposits of La Quina Amont (Charente, France) using luminescence methods. J. Hum. Evol. 109, 30–45.

Frouin, M., Guérin, G., Lahaye, C., Mercier, N., Huot, S., Aldeias, V., Bruxelles, L., Chiotti, L., Dibble, H.L., Goldberg, P., Madelaine, S., McPherron, S.J.P., Sandgathe, D., Steele, T.E., Turq, A.., 2017. New luminescence dating results based on polymineral fine grains from the Middle and Upper Palaeolithic site of La Ferrassie (Dordogne, SW France). Quatern. Geochronol. 39, 131–141.

Galbraith, R.F., Roberts, R.G., Laslett, G.M., Yoshida, H., Olley, J.M., 1999. Optical dating of single and multiple grains of quartz from Jinmium rock shelter, northern Australia: Part I, experimental design and statistical models. Archaeometry 41 (2), 339–364.

Gómez-Olivencia, A., Crevecoeur, I., Balzeau, A., 2015. La Ferrassie 8 Neandertal child reloaded: new remains and re-assessment of the original collection. J. Hum. Evol. 82, 107–126.

Gómez-Olivencia, A., Quam, R., Sala, N., Bardey, M., Ohman, J.C., Balzeau, A., 2018. La Ferrassie 1: new perspectives on a "classic" Neandertal." J. Hum. Evol. 117, 13–32.

Guérin, G., Mercier, N., 2011. Determining gamma dose rates by field gamma spectroscopy in sedimentary media: results of Monte Carlo simulations. Radia. Meas. 46, 190–195.

Guérin, G., Lebrun, B., Marchand, G., Philippe, A., 2022. Age-depth modelling and the effect of including–or not–shared errors across sets of OSL samples: the case study of Beg-er-Vil (Brittany, France). Quatern. Geochronol. 70, 101311.

Guérin, G., Frouin, M., Talamo, S., Aldeias, V., Bruxelles, L., Chiotti, L., Dibble, H. L., Goldberg, P., Hublin, J.-J., Jain, M., Lahaye, C., Madelaine, S., Maureille, B, McPherron, S. P., Mercier, N., Murray, A. S., Sandgathe, D., Steele, T. E., Thomsen, K. J., Turq, A., 2015. A multi-method luminescence dating of the Palaeolithic sequence of La Ferrassie based on new excavations adjacent to the La Ferrassie 1 and 2 skeletons. J. Archaeol. Sci. 58, 147–166.

Guérin, G., Christophe, C., Philippe, A., Murray, A.S., Thomsen, K.J., Tribolo, C., Urbanova, P., Jain, M., Guibert, P., Mercier, N., Kreutzer, S., Lahaye, C., 2017. Absorbed dose, equivalent dose, measured dose rates, and implications for OSL age estimates: introducing the Average Dose Model. Quatern. Geochronol. 41, 163–173.

Guérin, G., Lahaye, C., Heydari, M., Autzen, M., Buylaert, J. P., Guibert, P., Jain, M., Kreutzer, S., Lebrun, B., Murray, A.S., Thomsen, K.J., Urbanova, P., Philippe, A., 2021. Towards an improvement of optically stimulated luminescence (OSL) age uncertainties: modelling OSL ages with systematic errors, stratigraphic constraints. Geochronol. 3(1), 229–245.

Hajdas, I., Ascough, P., Garnett, M. H., Fallon, S. J., Pearson, C. L., Quarta, G., Spalding, K.L., Yamaguchi, H., Yoneda, M., 2021. Radiocarbon dating. Nat. Rev. Methods Primers 1(1), 1–26.

Hansen, V., Murray, A., Buylaert, J.P., Yeo, E.Y., Thomsen, K., 2015. A new irradiated quartz for beta source calibration. Radia. Meas. 81, 123–127.

Heim, J.-L., 1976. Les hommes fossiles de La Ferrassie. Archives de l'Institut de Paléontologie Humaine 35, Tome I. Masson, Paris.

Heim, J.-L., 1982a. Les enfants néandertaliens de La Ferrassie. Fondation Singer Polignac. Masson, Paris.

Heim, J.-L., 1982b. Les hommes fossiles de La Ferrassie. Archives de l'Institut de Paléontologie Humaine, 38, Tome II. Masson, Paris.

Heydari, M., Guérin, G., 2018. OSL signal saturation and dose rate variability: Investigating the behaviour of different statistical models. Radia. Meas. 120, 96–103.

Heydari, M., Guérin, G., Kreutzer, S., Jamet, G., Kharazian, M. A., Hashemi, M., Vahdati Nasab, H., Berillon, G., 2020. Do Bayesian methods lead to more precise chronologies? BayLum and a first OSL-based chronology for the Palaeolithic open-air site of Mirak (Iran). Quatern. Geochronol. 59, 101082.

Heydari, M., Guérin, G., Zeidi, M., Conard, N.J., 2021. Bayesian luminescence dating at Ghār-e Boof, Iran, provides a new chronology for Middle and Upper Paleolithic in the southern Zagros. J. Hum. Evol. 151, 102926.

Higham, T., Douka, K., Wood, R., Ramsey, C.B., Brock, F., Basell, L., Camps, M., Arrizabalaga, A., Baena, J., Barroso-Ruíz, C. Bergman, C. Boitard, C., Boscato, P., Caparrós, M., Conard, N.J., Draily, C., Froment, A., Galván, B., Gambassini, P., Garcia-Moreno, A., Grimaldi, S., Haesaerts, P., Holt, B., Iriarte-Chiapusso, M.-J., Jelinek, A., Jordá Pardo, J.F., Maíllo-Fernández, J.-M., Marom, A., Maroto, J., Menéndez, M., Metz, L., Morin, E., Moroni, A., Negrino, F., Panagopoulou, E., Peresani, M., Pirson, S., de la Rasilla, M., Riel-Salvatore, J., Ronchitelli, A., Santamaria, D., Semal, P., Slimak, L., Soler, J., Soler, N., Villaluenga, A., Pinhasi, R., Jacobi, R., 2014. The timing and spatiotemporal patterning of Neanderthal disappearance. Nature 512(7514), 306–309.

Higham, T.F., Jacobi, R.M., Ramsey, C.B., 2006. AMS radiocarbon dating of ancient bone using ultrafiltration. Radiocarb. 48(2), 179–195.

Hublin, J. J., Sirakov, N., Aldeias, V., Bailey, S., Bard, E., Delvigne, V., Endarova, E., Fagault, Y., Fewlass, H., Hajdinjak, M., Kromer, B., Krumov, I., Marreiros, J., Martisius, N.L., Paskulin, L., Sinet-Mathiot, V.,Meyer,

M., Pääbo, S., Popov, V. Rezek, Z., Sirakova, S., Skinner, M.M., Smith, G.M., Spasov, R., Talamo, S., Tuna, T., Wacker, L., Welker, F., Wilcke, A., Zahariev, N., McPherron, S.P., Tsanova, T., 2020. Initial Upper Palaeolithic *Homo sapiens* from Bacho Kiro cave, Bulgaria. Nature 581(7808), 299–302.

Huntley, D.J., Godfrey-Smith, D.I., Thewalt, M.L.W. 1985. Optical dating of sediments. Nature 313, 105–107.

Lanos, P., Philippe, A., 2018. Event Date Model: a robust Bayesian tool for chronology building. Commun. Stat. Appl. Methods 25(2), 131–157.

Lanos, P., Philippe, A., 2017. Hierarchical Bayesian modeling for combining dates in archeological context. J. Soc. fr. stat. 158(2), 72–88.

Maureille, B., Van Peer, P., 1998. Une donnée peu connue sur la sépulture du premier adulte de la Ferrassie (Savignac-de-Miremont, Dordogne). Paleo 10, 291–301.

Mellars, P., 1996. The Neanderthal Legacy: An Archaeological Perspective from Western Europe. Princeton University Press, Princeton.

Mellars, P.A., Bricker, H.M., Hedges, J.A.J, Gowlett, R.E.M., 1987. Radiocarbon accelerator dating of French Upper Palaeolithic sites. Curr. Anthropol. 28(1), 128–133.

Murray, A.S., Olley, J.M., 2002. Precision and accuracy in the optically stimulated luminescence dating of sedimentary quartz. Geochronometria 21, 1–16.

Murray, A., Arnold, L. J., Buylaert, J. P., Guérin, G., Qin, J., Singhvi, A. K., Smedley, R., Thomsen, K., 2021. Optically stimulated luminescence dating using quartz. Nat. Rev. Methods Primers 1(1), 1–31.

Pederzani, S., Aldeias, V., Dibble, H. L., Goldberg, P., Hublin, J. J., Madelaine, S., McPherron, S.P., Sandgathe, D., Steele, T.E., Turq, A., Britton, K., 2021. Reconstructing Late Pleistocene paleoclimate at the scale of human behavior: an example from the Neandertal occupation of La Ferrassie (France). Sci. Rep. 11(1), 1–10.

Peyrony, D. 1934. La Ferrassie: Moustérien, Périgordien, Aurignacien. In: Leroux, E., Préhistoire III, 151. Paris, pp. 1–92.

Philippe, A., Vibet, M., 2020. Analysis of archaeological phases using the R Package ArchaeoPhases. J. Stat. Softw. 93(1), 1–25.

Philippe, A., Guérin, G., Kreutzer, S., 2019. BayLum-An R package for Bayesian analysis of OSL ages: an introduction. Quatern. Geochronol. 49, 16–24.

Ramsey, C.B., 2009. Bayesian analysis of radiocarbon dates. Radiocarb. 51(1), 337–360.

Reimer, P., Austin, W.E.N., Bard, E., Bayliss, A., Blackwell, P.G., Ramsey C.B., Butzin, M., Cheng, H., Edwards, R.L., Friedrich, M., Grootes, P.M., Guilderson, T.P., Hajdas, I., Heaton, T.J., Hogg, A.G., Hughen, K.A., Kromer, B., Manning, S.W., Muscheler, R., Palmer, J.G., Pearson, C., van der Plicht, J., Reimer, R.W., Richards, D.A., Scott, E.M., Southon, J.R., Turney, C.S.M., Wacker, L., Adolphi, F., Büntgen, U., Capano, M., Fahrni, S., Fogtmann-Schulz, A., Friedrich, R., Köhler, P., Kudsk, S., Miyake, F., Olsen, J., Reinig, F., Sakamoto, M., Sookdeo, A., Talamo, S., 2020. The IntCal20 northern hemisphere radiocarbon age calibration curve (0–55 cal kBP). Radiocarb. 62(4), 725–757.

Singh, A., Thomsen, K. J., Sinha, R., Buylaert, J. P., Carter, A., Mark, D. F., Mason, P.J., Densmore, A.L. Murray, A.S., Jain, M., Paul, D., Gupta, S., 2017. Counter-intuitive influence of Himalayan river morphodynamics on Indus Civilisation urban settlements. Nature Comm. 8, 1–14.

Skov, L., Peyrégne, S., Popli, D., Iasi, L.N., Devièse, T., Slon, V., Zavala, E.I., Hajdinjak, M., Sümer, A.P., Grote, S., Mesa, A.B., Herráez, D.L., Nickel, B., Nagel, S., Richter, J., Essel, E., Gansauge, M., Schmidt, A., Korlević, P., Comeskey, D., Derevianko, A.P., Kharevich, A., Markin, S.V., Talamo, S., Douka, K., Krajcarz, M.T., Roberts, R.G., Higham, T., Viola, B., Krivoshapkin, A.I., Kolobova, K.A., Kelso, J., Meyer, M., Pääbo, S., Peter, B.M., 2022. Genetic insights into the social organization of Neanderthals. Nature 610, 519–525.

Slon, V., Mafessoni, F., Vernot, B., De Filippo, C., Grote, S., Viola, B., Hajdinjak, M., Peyrégne, S., Nagel, S., Brown, S., Douka, K., Higham, T., Kozlikin, M.B., Shunkov, M.V., Derevianko, A.P., Kelso, J., Meyer, M., Prüfer, K., Pääbo, S., 2018. The genome of the offspring of a Neanderthal mother and a Denisovan father. Nature 561(7721), 113-116.

Talamo, S., Hajdinjak, M., Mannino, M. A., Fasani, L., Welker, F., Martini, F., Romagnoli, F., Roberto Zorzin, R., Meyer, M., Hublin, J.J., 2016. Direct radiocarbon dating and genetic analyses on the purported Neanderthal mandible from the Monti Lessini (Italy). Sci. Rep. 6(1), 1–9.

Talamo, S., Aldeias, V., Goldberg, P., Chiotti, L., Dibble, H.L., Guérin, G., Hublin, J.-J., Madelaine, S., Maria, R., Sandgathe, D., Steele, T.E., Turq, A., McPherron, S.J.P., 2020. The new 14C chronology for the Palaeolithic site of La Ferrassie, France: the disappearance of Neanderthals and the arrival of *Homo sapiens* in France. J. Quatern. Sci. 35(7), 961–973.

Thomsen, K.J., Murray, A.S., Buylaert, J.P., Jain, M., Hansen, J.H., Aubry, T., 2016. Testing single-grain quartz OSL methods using sediment samples with independent age control from the Bordes-Fitte rockshelter (Roches d'Abilly site, Central France). Quatern. Geochronol. 31, 77–96.

Supplement 1: A Third Neanderthal Individual from La Ferrassie Dated to the End of the Middle Paleolithic

GUILLAUME GUÉRIN
Université Rennes, CNRS, Géosciences Rennes, UMR 6118, 35000 Rennes, FRANCE; guillaume.guerin@univ-rennes1.fr

VERA ALDEIAS
Interdisciplinary Center for Archaeology and Evolution of Human Behaviour (ICArEHB), FCHS, University of Algarve, Faro, PORTUGAL; vlaldeias@ualg.pt

FREDERIK BAUMGARTEN
Department of Physics, Technical University of Denmark, DTU Risø Campus, Roskilde, DENMARK; fhaba@dtu.dk

PAUL GOLDBERG
Institute for Archaeological Sciences, University of Tübingen, 72074 Tübingen, GERMANY; and, SEALS, University of Wollongong, Wollongong, NSW 2522, AUSTRALIA; paulberg@bu.edu

ASIER GÓMEZ-OLIVENCIA
Departement Geología, Universidad del País Vasco/Euskal Herriko Unibertsiatea (UPV/-EHU), Barrio Sarriena s/n, 48940 Leioa; Sociedad de Ciencias Aranzadi, Zorroagagaina 11, 20014 Donostia-San Sebastian; and, Centro UCM-ISCIII de Investigación sobre Evolución y Comportamiento Humanos, Avda. Monforte de Lemos 5 (Pabellón 14), 28029 Madrid, SPAIN; asiergo@gmail.com

CHRISTELLE LAHAYE
Archéosciences Bordeaux, UMR 6034 CNRS - Université Bordeaux Montaigne, Maison de l'archéologie, Esplanade des Antilles, 33607 Pessac cedex, FRANCE; christelle.lahaye@u-bordeaux-montaigne.fr

STÉPHANE MADELAINE
Musée national de Préhistoire, F-24620 Les Eyzies-de-Tayac; and, Université Bordeaux, CNRS, MC, PACEA UMR 5199, F-33600 Pessac, FRANCE; stephane.madelaine@culture.gouv.fr

BRUNO MAUREILLE
Université Bordeaux, CNRS, MC, PACEA UMR 5199, F-33600 Pessac, FRANCE; bruno.maureille@u-bordeaux.fr

ANNE PHILIPPE
Jean Leray Laboratory of Mathematics (LMJL), UMR 6629 CNRS - Université de Nantes, Nantes, FRANCE; anne.philippe@univ-nantes.fr

DENNIS SANDGATHE
Human Evolution Studies Program and Department of Archaeology, Simon Fraser University, Burnaby, CANADA; dmsandga@gmail.com

SAHRA TALAMO
Department of Chemistry, University of Bologna, Bologna, ITALY; sahra.talamo@unibo.it

KRISTINA JØRKOV THOMSEN
Department of Physics, Technical University of Denmark, DTU Risø Campus, Roskilde, DENMARK; krth@dtu.dk

ALAIN TURQ
Musée national de Préhistoire, F-24620 Les Eyzies-de-Tayac; and, Université Bordeaux, CNRS, MC, PACEA UMR 5199, F-33600 Pessac, FRANCE; alain.turq@orange.fr

ANTOINE BALZEAU
Équipe de Paléontologie Humaine, UMR 7194, CNRS, Département Homme et environnement, Muséum national d'Histoire naturelle, Musée de l'Homme, 17 Place du Trocadéro, 75016 Paris, FRAMCE; and, Department of African Zoology, Royal Museum for Central Africa, Tervuren, BELGIUM; antoine.balzeau@mnhn.fr

SUPPLEMENT 1

Fig. S1. Block of sediment sampled for OSL dating (left). The label reads '*Fragments de la gangue de LA FERRASSIE 1*' (Fragments of the matrix of LA FERRASSIE 1). Observations conducted by one of us (PG) with a hand-lens tend to confirm the hypothesis that this block of sediment originates from Layer 5.

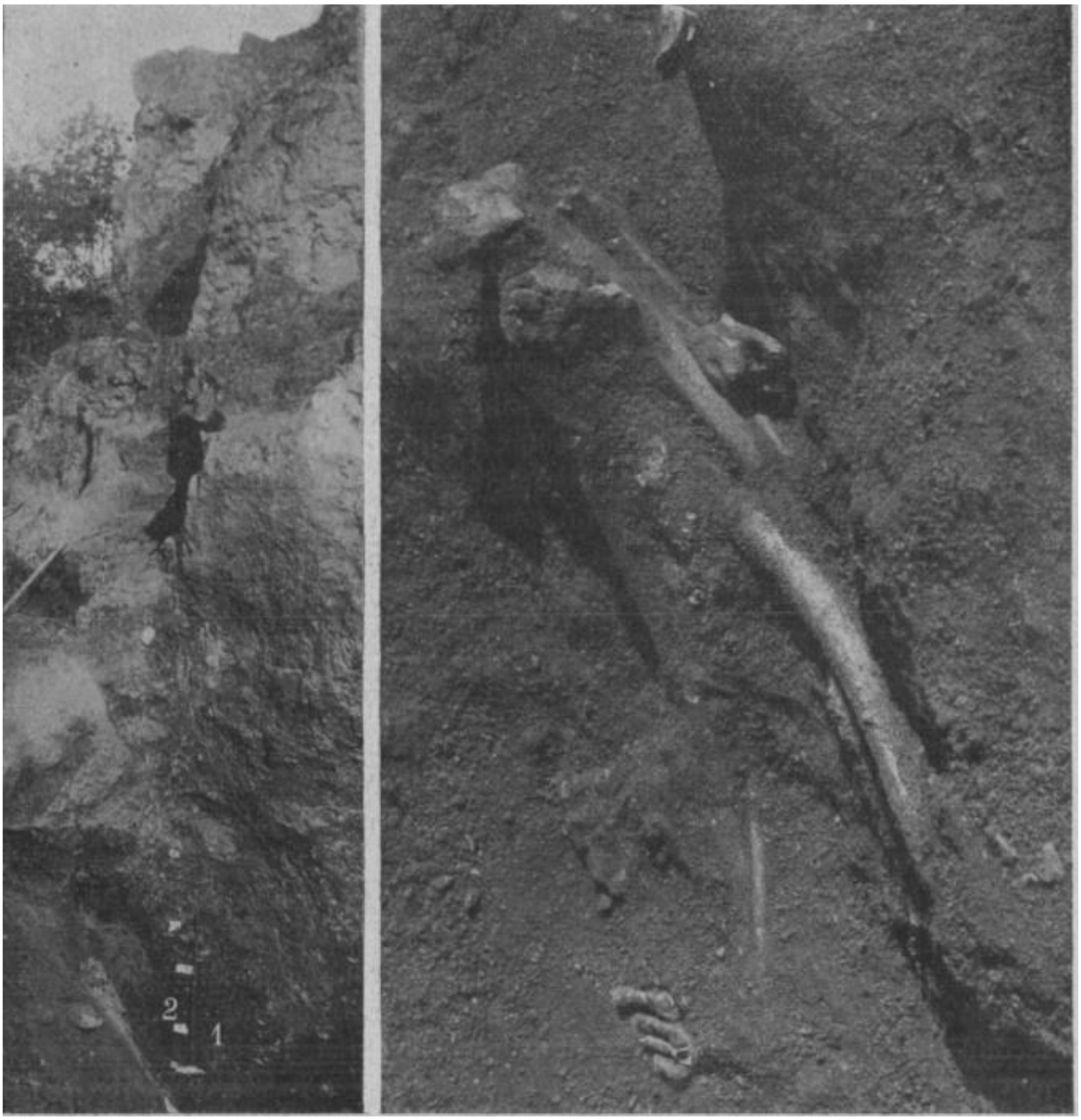

Fig. S2. Reproduction of Figures 28 and 29 of Capitan and Peyrony (1912). Their caption can be translated as: Fig. 28 (left) – small squares indicate layer separation; 1, position of the first skeleton; 2, emplacement of the second skeleton. Fig. 29 (right). Members of the second skeleton found in the Mousterian layer […].

Based on Figure 28, on may see that the skeletons were found close to the layer lying just above (our layer 6) and that, since LF can most likely be attributed to Layer 5 based on sedimentological observations (Guérin et al., 2015), it is tempting to also attributed LF1 to Layer 5. That being said, Capitan and Peyrony did not distinguish between our Layers 4 and 5, so one has to remain cautious.